Chapter 11

MOBY, A Radiometric Buoy for Performance Monitoring and Vicarious Calibration of Satellite Ocean Color Sensors: Measurement and Data Analysis Protocols

Dennis K. Clark[1], Mark A. Yarbrough[2], Mike Feinholz[2], Stephanie Flora[2], William Broenkow[2], Yong Sung Kim[3], B. Carol Johnson[4], Steven W. Brown[4], Marilyn Yuen[1], and James L. Mueller[5]

[1]*NOAA National Environmental Satellite Data Information Service, Suitland, Maryland*
[2]*Moss Landing Marine Laboratory, California*
[3]*Data Systems Technologies, Inc., Rockville, Maryland*
[4]*National Institute of Standards and Technology, Gaithersburg, Maryland*
[5]*Center for Hydro-Optics and Remote Sensing, San Diego State University, California*

11.1 INTRODUCTION

The Marine Optical Buoy (MOBY) (Clark *et al.* 1997) is the centerpiece of the primary ocean measurement site for calibration of satellite ocean color sensors based on independent *in situ* measurements. Since late 1996, the time series of normalized water-leaving radiances $L_{WN}(\lambda)$ determined from the array of radiometric sensors attached to MOBY are the primary basis for the on-orbit calibrations of the USA Sea-viewing Wide Field-of-view Sensor (SeaWiFS), the Japanese Ocean Color and Temperature Sensor (OCTS), the French Polarization Detection Environmental Radiometer (POLDER), the German Modular Optoelectronic Scanner on the Indian Research Satellite (IRS1-MOS), and the USA Moderate Resolution Imaging Spectrometer (MODIS). The MOBY vicarious calibration $L_{WN}(\lambda)$ reference is an essential element in the international effort to develop a global, multi-year time series of consistently calibrated ocean color products using data from a wide variety of independent satellite sensors.

A longstanding goal of the SeaWiFS and MODIS (Ocean) Science Teams is to determine satellite-derived $L_{WN}(\lambda)$ with a relative combined standard uncertainty[1] of 5 % (Chapter 1). Other satellite ocean color projects and the Sensor Intercomparison for Marine Biology and Interdisciplinary Oceanic Studies (SIMBIOS) project have also adopted this goal, at least implicitly. Because water-leaving radiance contributes at most 10 % of the total radiance measured by a satellite sensor above the atmosphere (Gordon 1997), a 5 % uncertainty in $L_{WN}(\lambda)$ implies a 0.5 % uncertainty in the above-atmosphere radiance measurements. This level of uncertainty can only be approached using "vicarious-calibration" approaches as described below. In practice, this means that the satellite radiance responsivity is adjusted to achieve the best agreement, in a least-squares sense, for the $L_{WN}(\lambda)$ results determined using the satellite and the independent optical sensors (*e.g.* MOBY). The end result of this approach is to implicitly absorb unquantified, but systematic, errors in the atmospheric correction, incident solar flux, and satellite sensor calibration into a single correction factor to produce consistency with the *in situ* data (see *e.g.* Gordon 1981, 1987, 1988).

Clearly, the combined standard uncertainty of the *in situ* $L_{WN}(\lambda)$ determinations must be less than 5 % if the stated uncertainty goal is to be approached. The uncertainty budget of MOBY $L_{WN}(\lambda)$ determinations may be divided into environmental and radiometric factors. Environmental factors include uncertainties

[1] All uncertainties in this document are standard uncertainties, unless noted otherwise. Standard uncertainty is the uncertainty of the result of a measurement expressed as a standard deviation (Taylor and Kuyatt 1994).

due to radiance and irradiance fluctuations associated with surface waves and platform motions during the radiometric measurements, and with extrapolation of upwelling radiance measurements from depths of 1 m or more to, and through, the sea surface. The uncertainties associated with these ambient conditions have been shown to be less than, but approaching, 5 % for upwelled radiance (Siegel *et al.* , 1995; Hooker and Maritorena, 2000). Radiometric uncertainty components associated with instrument characterization, calibration and stability, *i.e.* the radiance measurements *per se*, must be summed in quadrature to yield the combined standard uncertainty of the MOBY $L_{WN}(\lambda)$ determinations.

The estimated combined standard uncertainty of MOBY radiance measurements is between 4 % and 8 % (Clark *et al.* 2001). This estimate is based on uncertainties of MOBY calibrations at less than 3 %, changes in pre- and post-deployment calibrations ranging from 1 % to 6 %, radiometric stability tests during deployments using internal reference sources that show changes less than 1 %, and diver-deployed external reference lamp responses that are stable within less than 3 % (the estimated uncertainty of the method) (Clark *et al.* 2001). The 8 % upper limit on the combined standard uncertainty estimate does not include preliminary results of recently undertaken stray light characterization of the MOBY spectrographs, which indicate systematic stray light offsets in $L_{WN}(\lambda)$ may have approximate magnitudes of +5 % and -3 % at blue and green wavelengths respectively (Sects. 11.4 and 11.8 below, and Clark *et al.* 2001). Once the stray light characterization is completed on all MOBY spectrographs, the entire MOBY $L_{WN}(\lambda)$ time series will be reprocessed with an expected combined standard uncertainty of less than 5 %. Variations in the measurement environment may add additional uncertainty.

The nature of, and data requirements for, vicarious calibration of a satellite ocean color sensor are briefly described in Chapter 1 (Sect. 1.5), and in more detail by Gordon (1981, 1987, 1988, 1997), Gordon *et al.* (1983), Evans and Gordon (1994), and Clark *et al.* (1997). A critical element of the procedure is the ability to monitor a satellite sensor's performance at daily to weekly intervals by comparing its derived $L_{WN}(\lambda)$ with concurrently derived *in situ* $L_{WN}(\lambda)$ meeting the uncertainty criteria described above. The most direct way of measuring $L_{WN}(\lambda)$ on a continuing daily basis over periods of several years is to utilize a specially designed array of radiometers mounted on a moored buoy. This buoy must be designed to mount the optical collectors well away from platform shading and reflections, artifacts similar to ship shadow, as discussed in Chapter 10 (Sect. 10.2). To minimize uncertainties due to extrapolation of upwelling radiance $L_u(z,\lambda)$ to the sea surface, the buoy must be moored at a location with consistently transparent case 1 waters and with negligible mesoscale to sub-mesoscale spatial variability. To assure frequent occurrences of matched satellite and buoy measurements, the site must be cloud free throughout most of the year. The mooring must be located close to an island based sun photometer and sky radiance sensor to allow concurrent determinations of aerosol optical thickness and sky radiance distribution. On the other hand, the atmospheric conditions at the mooring location must not be significantly influenced by the island's wake. Extraordinary calibration maintenance procedures are needed to assure low uncertainties in the buoy's radiometric measurements. In addition, comparative shipboard measurements must be made near the buoy to check the radiometric stability of its instrumentation, to determine spatial variability surrounding the buoy location, and to develop and validate bio-optical algorithms. Some of these measurements can be made during cruises staged to replace the mooring at 3 to 4 month intervals, but dedicated cruises of 1 to 2 week duration are also required. The logistical demands of buoy maintenance, calibration activities, deployment and relief, and ship support operations strongly argue for placing the buoy conveniently near a permanent support facility. The locations of the MOBY mooring, near the island of Lanai, and the associated support facilities in Honolulu, Hawaii closely satisfy all of the above conditions.

The radiometric measurements at a primary reference site for vicarious calibration of satellite ocean color sensors differ in several aspects from the radiometric in-water profiling methods described in the Chapter 10. A primary reference data set must consist of *in situ* determinations of band-averaged $L_{WN}(\lambda)$'s that reproduce the spectral response functions of each satellite sensor's bands with more accuracy than can be realized using off the shelf radiometers. The need for flexibility in the choice of spectral response weighting functions used to determine band-averaged $L_{WN}(\lambda)$ imposes a requirement for full-spectrum measurements with resolutions <1 nm. Instead of measuring radiometric profiles resolved at several samples per m (Chapter 10, Sect. 10.2), downwelling irradiance $E_d(z,\lambda)$ and upwelling radiance $L_u(z,\lambda)$ can be measured on a buoy at only a few fixed depths, which complicates the problem of accurately determining $L_u(0^-,\lambda)$ (just below the sea surface).

To be affordable, a moored array must typically be deployed and operated semi-autonomously for periods of 3 to 4 months. Provisions to assure radiometric stability through these extended period operations should include, as a minimum, pre- and post-deployment calibrations of all radiometers, combined with continuous monitoring of on-board light sources of known stability. Moreover, instruments suspended in seawater for periods of this duration experience fouling by biological organisms that, if not countered effectively using antifouling methods and frequent cleaning by divers, seriously degrade the performance of optical sensors. Affordable servicing and maintenance during each deployment is limited to *circa* monthly visits by divers to clean instruments, check sensor calibrations against portable underwater lamp sources, and perform minimal maintenance.

Because of these uniquely different measurement requirements, platform related geometry, instrument characteristics, and operational conditions, the protocols applying to the MOBY instruments and methods of measurement and data analysis are presented separately in the present chapter. Where appropriate, certain protocols will be defined and described by reference to other chapters. This chapter documents the protocols used by the MOBY Operations Team to measure and derive the MOBY data sets that consist of the $L_{WN}(\lambda)$ time series. The information is intended as background for those wishing to apply this data to validate water-leaving radiances from one or more satellite ocean color sensors.

11.2 THE MOBY PRIMARY VICARIOUS CALIBRATION SITE

The primary components of the MOBY vicarious calibration site are located as shown in Fig. 11.1. A MOBY is continuously moored approximately 20 km west of the island of Lanai in 1200 m of water. During prevailing trade wind conditions, this location is sheltered in the lee of the island, yet it is far enough offshore to minimize atmospheric perturbations associated with the island's wake. CIMEL[2] sun photometers on Lanai and Oahu, operated by the Aerosol Robotic Network (AERONET) Project (Chapters 7 and 14), provide time series measurements of aerosol optical thickness and sky radiance distributions that are required to reduce the uncertainty budgets of atmospheric correction models used during vicarious calibration analyses. The MOBY Operation Site, located at the University of Hawaii (UH) Marine Facility in Honolulu, is staffed full time by personnel from the Moss Landing Marine Laboratory (MLML) for buoy maintenance, instrument maintenance and calibration, and for staging buoy relief and bio-optical sampling cruises. The UH's research vessels are used for cruises to support buoy deployments (L-series cruises identified in Table 11.1), Marine Optical Characterization Experiments (MOCE-series), and interim maintenance and quality control operations. During the MOCE and some L-series cruises (Table 11.1), *in situ* bio-optical measurements are made to validate MOBY $L_{WN}(\lambda)$ determinations, to characterize spatial variability near the mooring, and to develop and validate bio-optical algorithms. A subset of the MOBY data is transmitted, in real time via cellular telephone, to the MLML in California. The MOBY data are processed at MLML to produce and extract appropriately weighted band-averaged $L_{WN}(\lambda)$'s for SIMBIOS and SeaWiFS Project Offices at the National Aeronautics and Space Administration (NASA) Goddard Space Flight Center (GSFC), and/or to the MODIS Team at the University of Miami.

MOBY and the Marine Optical System (MOS)

MOBY is a 12 m spar buoy (including the lower instrument bay) uniquely designed as an optical bench for measurements of $E_d(z,\lambda)$ and $L_u(z,\lambda)$ at depths of 1 m, 5 m, 9 m, and 12 m (Fig. 11.2). The features of MOBY are summarized in Table 11.2. Fig. 11.3 is a schematic illustration of the MOBY system's sensors, operations and communications, while the mechanical layouts of the upper and lower instrument bays are illustrated in Fig. 11.4 and Fig. 11.5, respectively. The MOBY spar is tethered to a second surface buoy, which is slack moored, *i.e.* isolated by subsurface floats, to an anchor on the sea floor (Fig. 11.6). Sensors for wind speed, wind direction, air temperature, relative humidity, and barometric pressure are mounted on the main mooring buoy.

[2] Certain commercial equipment, instruments, or materials are identified in this document to foster understanding. Such identification does not imply recommendation or endorsement by the National Institute of Standards and Technology, nor does it imply that the materials or equipment identified are necessarily the best available for the purpose.

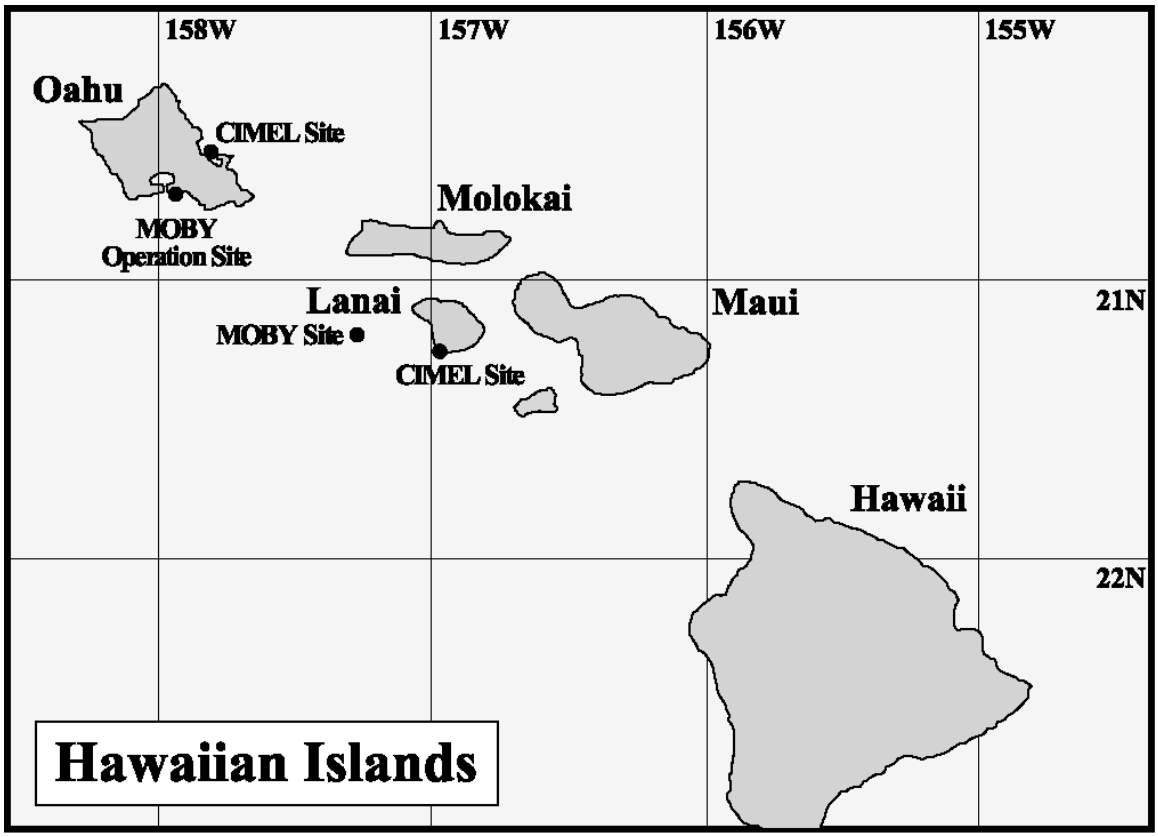

Figure 11.1: Chart showing locations of the MOBY mooring, the two CIMEL robotic sun photometers on Oahu and Lanai, cell phone relay stations used for data communications, and the MOBY Operations Site in Honolulu, Hawaii.

The Marine Optical System (MOS), the heart of MOBY, consists of two single-grating CCD spectrographs connected via an optical multiplexer and fiber optic cables to the $E_d(z,\lambda)$ and $L_u(z,\lambda)$ optical heads mounted at the ends of the buoy's 3 standoff arms (Fig. 11.2 and Fig. 11.3). To provide low-loss transmission at ultraviolet wavelengths, 1 mm diameter silica fiber-optic cables are used to connect the optical heads to MOS. $L_u(12,\lambda)$, at z = 12 m, is measured through a window in the bottom of the MOS housing itself. A seventh fiber optic cable connects a surface irradiance $E_s(\lambda)$ cosine collector, mounted at the top of the MOBY above-water mast, to the spectrographs. Each pair of in-water optical heads is mounted on a standoff arm to minimize radiometric artifacts due to shadows or reflections from the buoy. To minimize self-shading by the $L_u(z,\lambda)$ radiometer (Chapter 10, Sect. 10.4; Gordon and Ding 1992), the underwater housings for the optical heads are very small in diameter (7 cm).

The principal characteristics of MOS are summarized in Table 11.3. The MOS system elements and optical layout are illustrated schematically in Fig. 11.7 and Fig. 11.8, respectively. Light from an $L_u(z,\lambda)$, $E_d(z,\lambda)$, or $E_s(\lambda)$ head enters the spectrograph package via its fiber optic cable and the multiplexer, is directed to a dichroic mirror that reflects light at wavelengths between 350 nm and 630 nm into one (blue) grating spectrograph, and transmits wavelengths greater than 630 nm to the other (red) spectrograph. The MOS spectrograph package is mounted in MOBY's lower instrument bay (Fig. 11.5), at a depth of approximately 12 m, primarily to isolate the package from the shock and vibration that surface waves inflict on the upper instrument bay. The deeper location also facilitates heat dissipation from the thermoelectric coolers used to maintain the operating temperature of the CCD arrays, and $L_u(12,\lambda)$ may be measured through the MOS optical window at the very bottom of the MOBY spar. Even more critically,

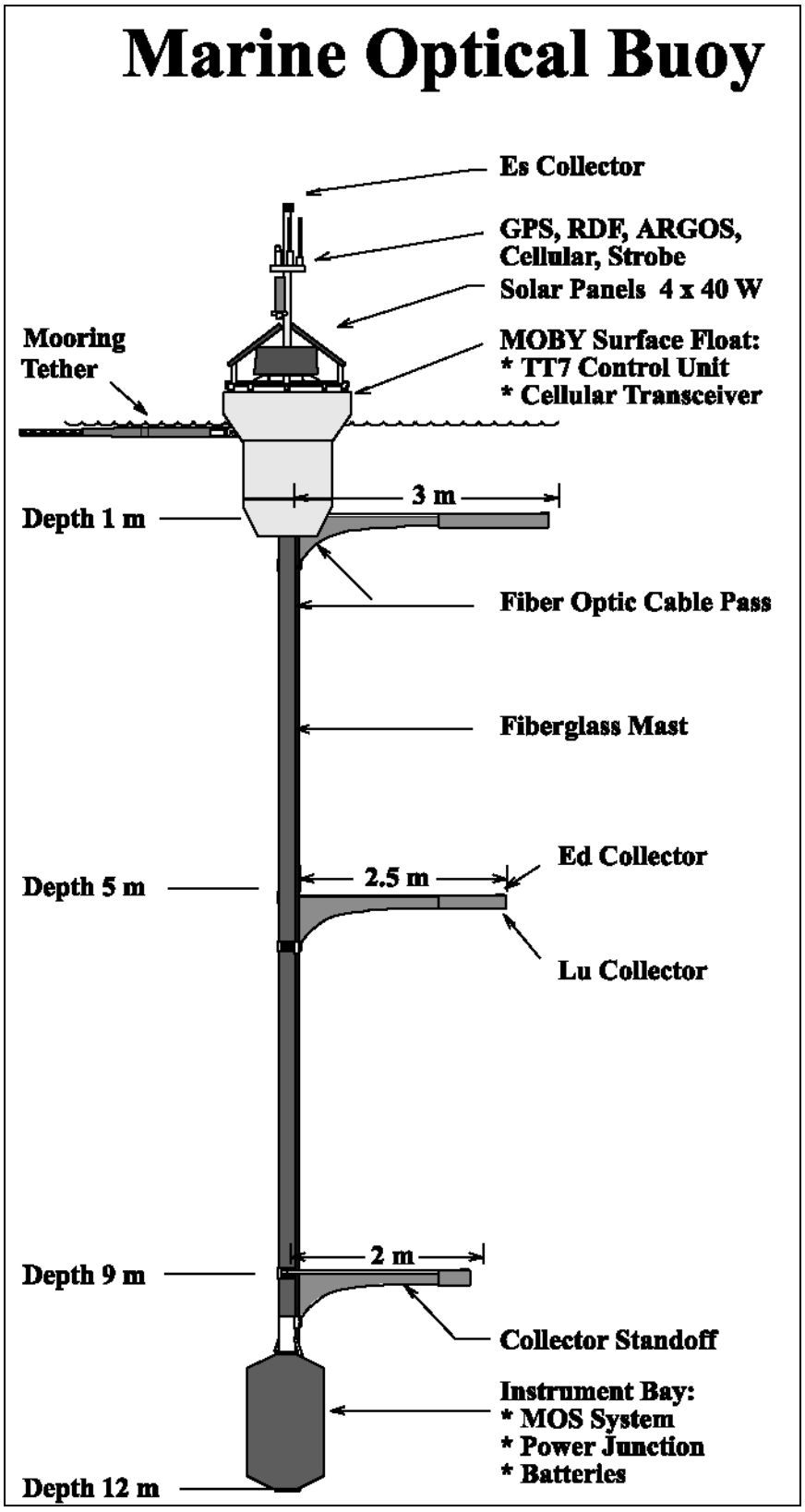

Figure 11.2: The Marine Optical Buoy (MOBY).

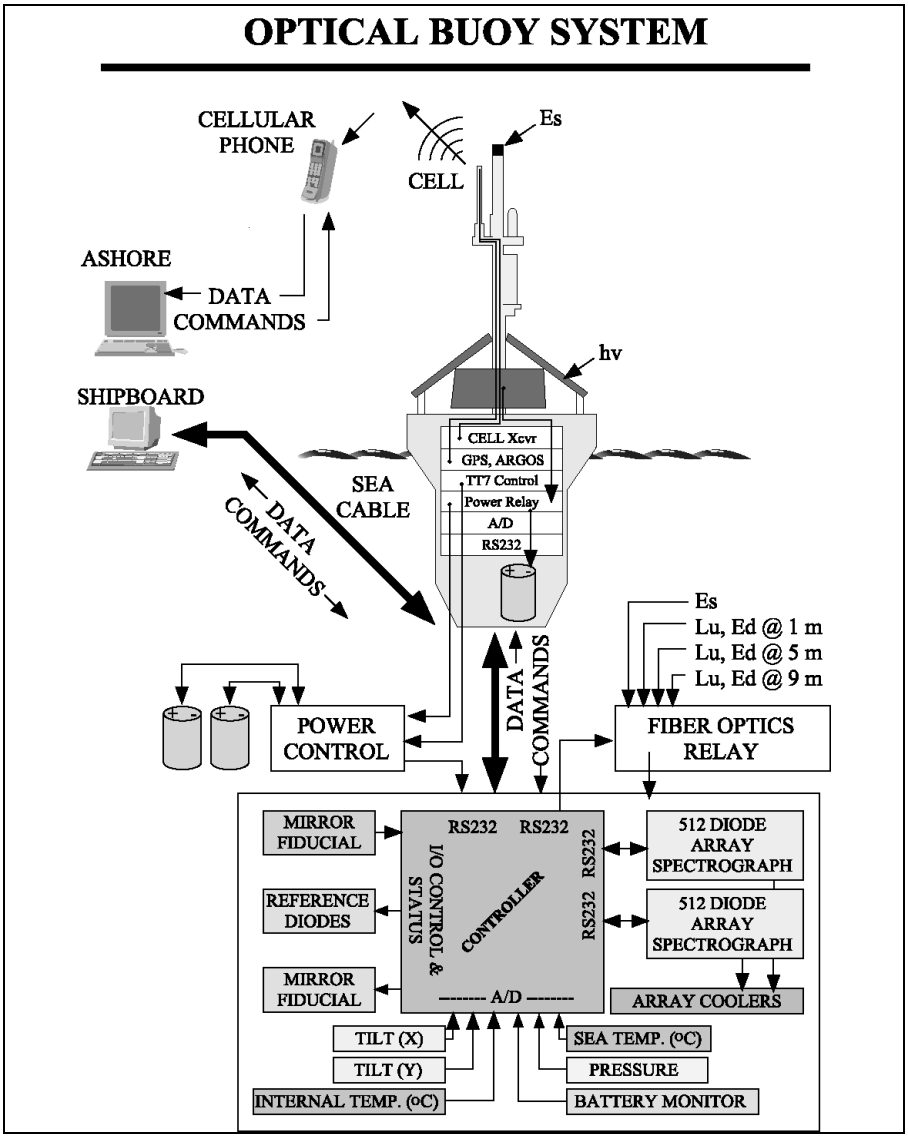

Figure 11.3: A schematic overview of the MOBY system elements.

the high current draw of the MOS requires that it be located close to the batteries, which themselves must be placed at the bottom of the spar to act as stabilizing ballast.

The elements defining the spectral radiometric characteristics of each of the spectrographs are the entrance slit, holographic grating, and cooled CCD detector array (Fig. 11.8). For the blue spectrograph (350 nm to 630 nm), the full-width at half-maximum (FWHM) bandpass of the spectral slit response function centered at any given wavelength is approximately 2 nm, and the 512 element detector array is designed to sample at approximately a 0.6 nm interval. The MOS was designed with such high spectral resolution to support vicarious calibrations of a variety of different satellite ocean color sensors (Appendix A). By measuring *in situ* spectra of $L_u(\lambda,z)$ at this resolution, it is practical to compute band-averaged values of $L_{WN}(\lambda)$ that are appropriately weighted for any of these satellite ocean color sensors.

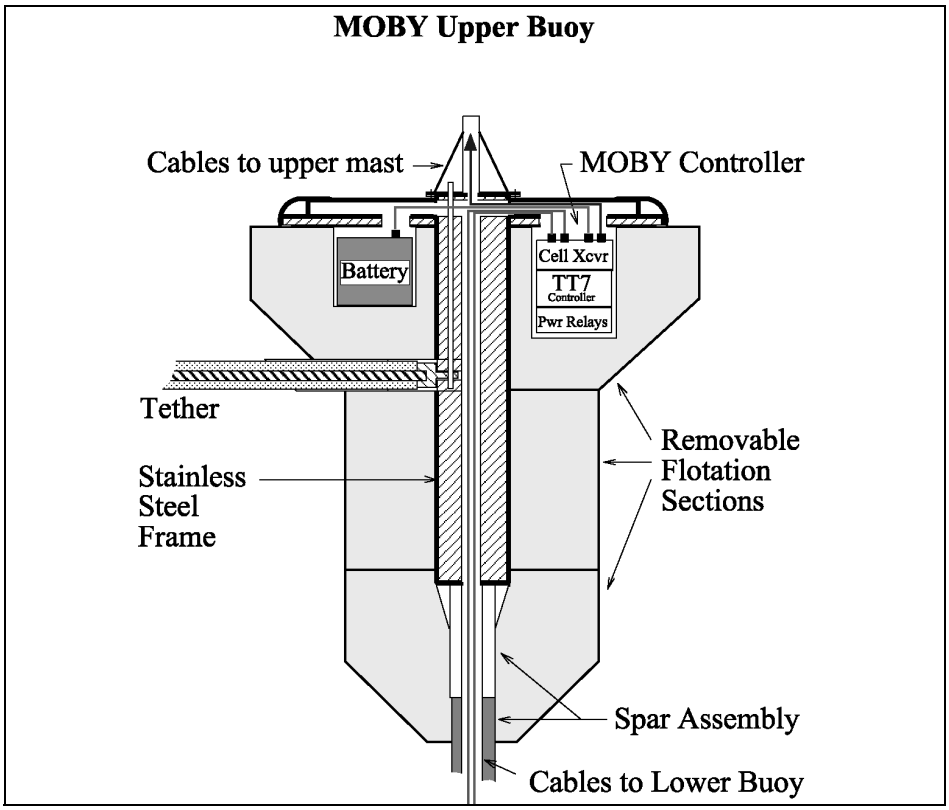

Figure 11.4: The MOBY flotation and upper instrument bay assembly.

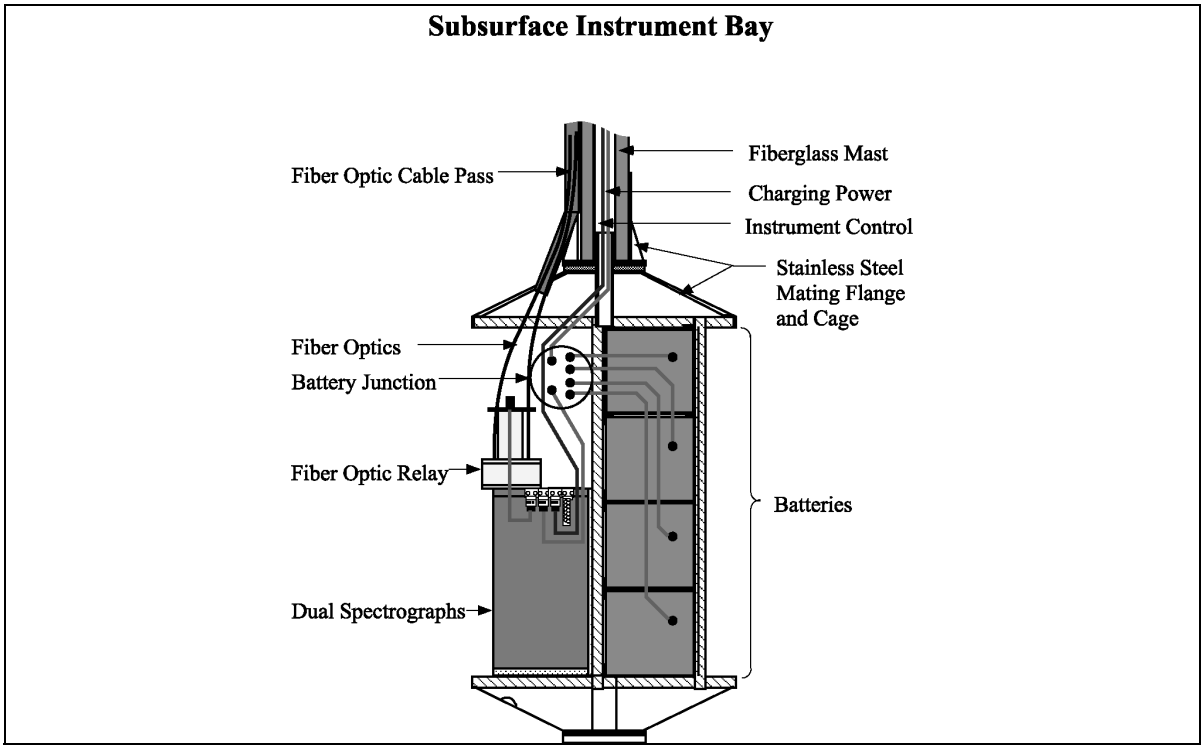

Figure 11.5: A schematic diagram illustrating the mechanical layout of the subsurface instrument and battery bay on MOBY.

Ancillary Measurements on MOBY

The principal navigation (latitude and longitude) and UTC (Universal Time, Coordinated) clock reference are determined from the Global Positioning System (GPS) receiver mounted in the MOBY upper instrument bay (Fig. 11.3 and Table 11.2). A secondary navigational position is provided by the System ARGOS transmitter, which is also installed in the upper bay (Fig. 11.3) and provides frequent MOBY position updates as a precaution against losing the buoy should the mooring fail. On two occasions, in fact, the MOBY array did break away from its moorings and was recovered safely thanks to the ARGOS tracking capability. Additional ancillary sensors are installed in the MOS package:

- Internal housing and CCD array temperatures are measured as indicators of performance quality, and may be used in applying radiometric calibration factors to the data.
- A high precision pressure transducer is installed on the top radiometric arm (Fig. 11.2) to determine depth variations $[z(t) - z_p]$ about its nominal reference depth z_p (fixed by its location on the spar) during each radiometric measurement sequence. A separate temperature sensor monitors the temperature of the pressure transducer, to minimize uncertainties in the depth determinations.
- Tilt sensors within the MOS package are used to determine the 2-axis orientation (pitch and yaw) of the MOBY spar relative to the local vertical. A flux gate compass, also installed within the MOS package, is used to determine the direction (magnetic) in which the radiometric sensor arms extend out from the spar. The relative angle between the spar pointing azimuth and the solar azimuth are used to detect measurement geometries in which the irradiance and radiance collectors may be influenced by shadows, or reflections, from the main MOBY structure.

Mooring Buoy Measurements

Sensors mounted on the mast of the mooring buoy measure wind velocity, surface barometric pressure, air temperature, and relative humidity (Fig. 11.6). Also, near surface sensors on this buoy measure water temperature and conductivity, and chlorophyll *a* fluorescence.

Data Communications

Data from the MOS and other sensors mounted on MOBY are assembled into data records, and annotated with time, latitude and longitude as based on GPS input, by the Tattletale[2] (Model TT7) microcomputer installed in the upper instrument bay (Table 11.2, Fig. 11.3 and Fig. 11.4). Data records are stored on hard disk for download when the MOBY is recovered and replaced at the end of a deployment. The microcomputer also transmits the data records over the cellular phone link to MLML in California. Normally, 99 % of the data are recovered via telemetry. Data from the meteorological sensors on the mooring buoy are similarly processed autonomously by a microcomputer. All data records are stored on hard disk and are downloaded once daily.

11.3 MOBY OPERATIONS AND MEASUREMENT METHODS

Deployment Schedule and Methods

There are two complete MOBY systems, one of which is moored and operational at any given time. The history of MOBY deployments, and key events associated with each, are summarized in Table 11.4. The typical duration of a single mooring deployment is between 3 and 4 months. During this period, the other MOBY is maintained and refurbished and its MOS recalibrated. At approximately monthly intervals during a deployment, the Operations Team visits the MOBY mooring site using a small boat launched from the island of Maui. During these interim visits, divers clean the optical collectors and use a specially designed underwater lamp reference source to check the radiometric stability of the deployed MOS (Sect. 11.4). During these “interim-servicing” cruises, water samples are filtered for phytoplankton pigment analyses, for comparison with pigment concentration determinations using the MOBY radiometric measurements. These pigment concentration comparisons are made to validate the pigment algorithms associated with the various satellite ocean color sensors.

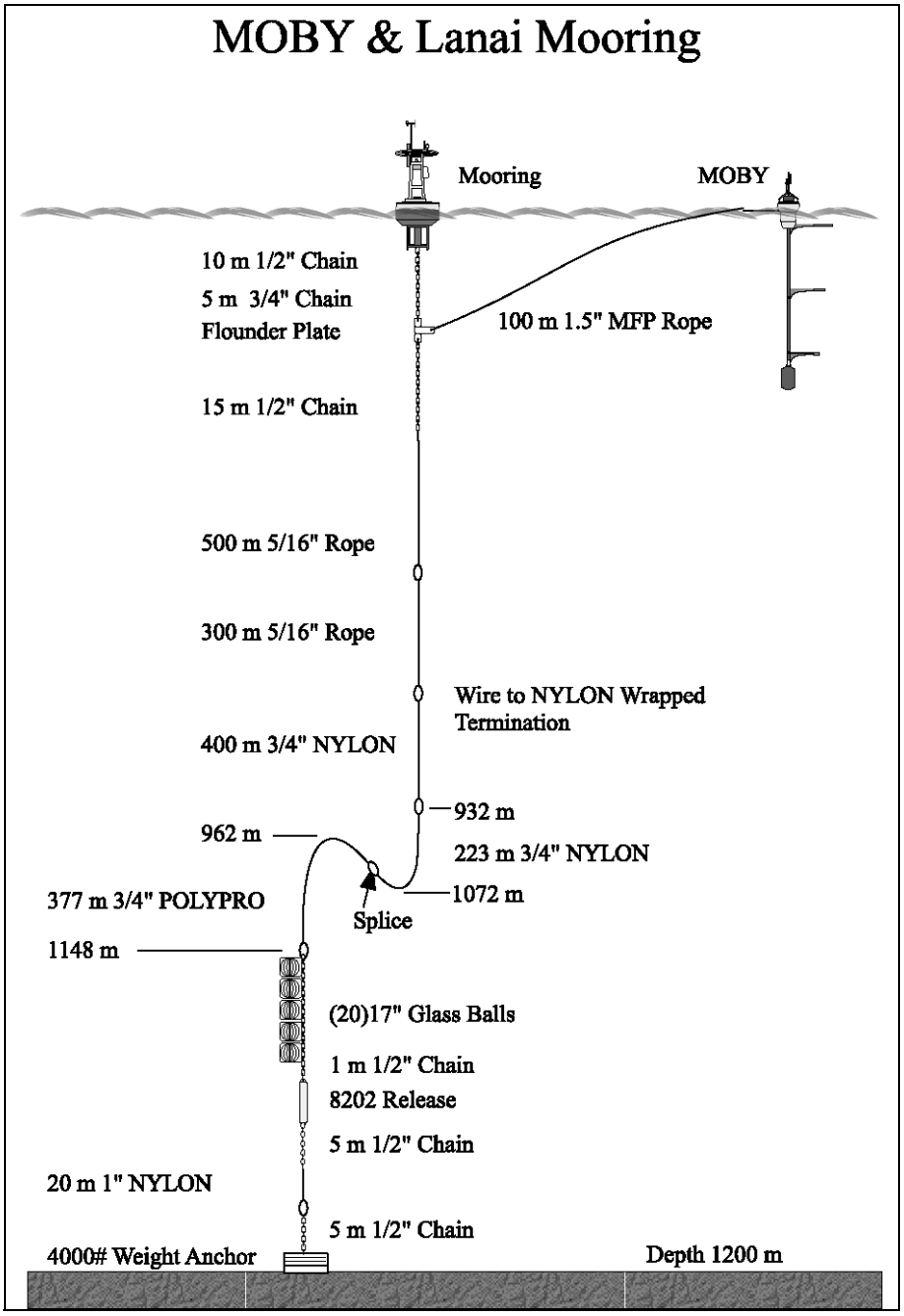

Figure 11.6: The MOBY mooring configuration.

When the time comes to exchange the MOBY systems, the replacement buoy is loaded aboard a research vessel and transported to the mooring site. On arriving at the site, the recalibrated and refurbished replacement MOBY is first deployed and set adrift (Fig. 11.9). Divers release the tether connecting the moored MOBY to the mooring buoy. The replacement buoy is then towed into position by the divers

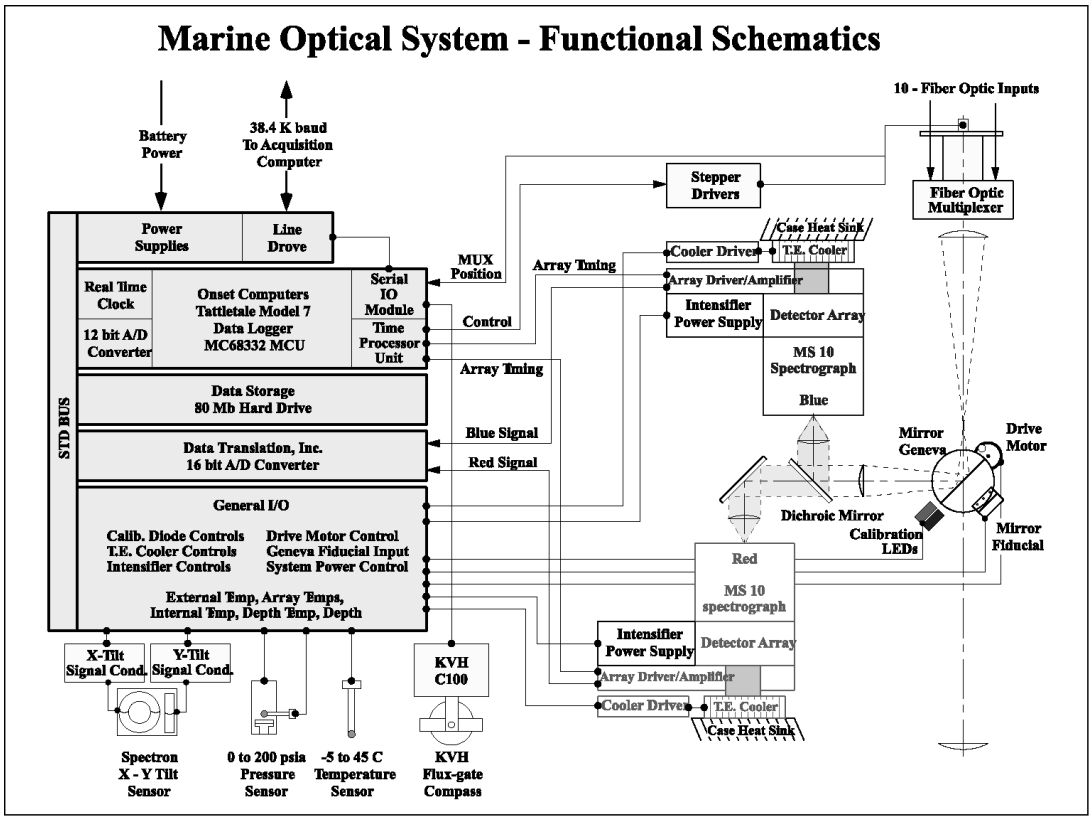

Figure 11.7: A schematic diagram of the MOS functional elements.

(operating from a support boat) and connected to the mooring. When possible, in-water radiometric measurements are made with both MOBY systems as a final check on the stability of the recovered system. Finally, the recovered MOBY is secured aboard the ship for its return to the MOBY Operations Site in Honolulu. The entire mooring (Fig. 11.6) is replaced at approximately 1-year intervals (Table 11.4). On these occasions, the acoustic release (Fig. 11.6) is activated to free the mooring line and its flotation from its anchor. A new anchor and surface mooring buoy are deployed, and a MOBY is tethered to it.

MOCE and Other Validation Shipboard Operations

On some of the MOBY replacement cruises ("L-cruises" in Table 11.1), additional ship time is used to make "Required" and "Highly Desired" radiometric and bio-optical measurements (Chapter 3, Table 3.1), both for radiometric validation of the MOBY and satellite ocean color sensor measurements, and for algorithm development and validation.

Complementing the MOBY project are the MOCE cruises, which are carried out primarily to support vicarious calibration and validation of satellite ocean color sensors. The MOCE team is comprised of scientists from the National Oceanic and Atmospheric Administration/National Environmental Satellite Data Information Service (NOAA/NESDIS), MLML, San Diego State University, and the University of Miami (Florida). MOCE cruises, which are typically between 10 and 30 days in duration, have been conducted in the general vicinity of the MOBY site and off the west coast of North America (Table 11.1).

Measurements acquired during the MOCE cruises are generally more extensive than those made during the "L-cruises". As an example, measurements made during MOCE-5 are listed in Table 11.5, which includes all of the "Required", nearly all of the "Highly Desired" and some of the "Specialized Measurements" categories of variables listed in Table 3.1 (Chapter 3). Protocols for most of these measurements and analyses conform to those described elsewhere in this document. However, protocols

are not provided elsewhere for two of the specialized measurements listed in Table 11.5, "Instrument Self-Shading" and "Particle Size Distribution", nor are measurements of these variables identified in Chapter 3.

The effects of instrument self-shading on upwelling radiance and irradiance measurements are discussed briefly in Chapter 4 (Sect. 4.2), and provisional protocols (based on Gordon and Ding 1992) for removing self-shading effects from measurements are described in Chapter 10 (Sect. 10.4). Direct measurements of the self-shading phenomenon are made during MOCE cruises (Table 11.5) to test the predictions of Gordon and Ding (1992) and determine relative uncertainties under a variety of ambient illumination conditions. A Fiber Optic Spectrometer (FOS) was developed using two modified American Holographic AH4000 series dual-beam spectrometers, one configured for radiometric measurements spanning the wavelength range from 375 nm to 725 nm at 5 nm resolution, and the other from 600 nm to 1100 nm at 10 nm resolution. The spectrometers are placed in a pressure housing and are coupled by fiber-optic leads to upwelling radiance and downwelling irradiance collectors that are located approximately 1 m away to minimize shading and reflection effects. The upwelling radiance probe is ~5 cm in diameter, and the self-shading effect is varied by attaching discs of increasing diameter to it.

Particle size distributions are measured using a commercial (Spectrex) laser particle counter. Particle counts, binned by size, are determined by measuring the magnitude of reflections from particles in a small working volume of water illuminated by a Helium-Neon diode (670.8 nm) LASER. The working volume, which is embedded in a 100 ml water sample, and its geometry are defined by the optical elements of the instrument. The water sample is agitated with a magnetic stirrer to keep particles in suspension during the measurements. The protocols used for determining particle size distributions are those provided by the manufacturer of the Spectrex, which claim to resolve particle sizes as small as 1 μm. On the other hand, the assumptions underlying the method are that the individual particles are separated by distances large compared to the wavelength of illumination, and that particle diameters are at least 5 times larger than the wavelength, so that particle reflection is governed by geometric optics. Other investigators have used the Spectrex instrument to measure particle size distributions, but a community consensus has yet to be developed for protocols related to this measurement and its interpretation.

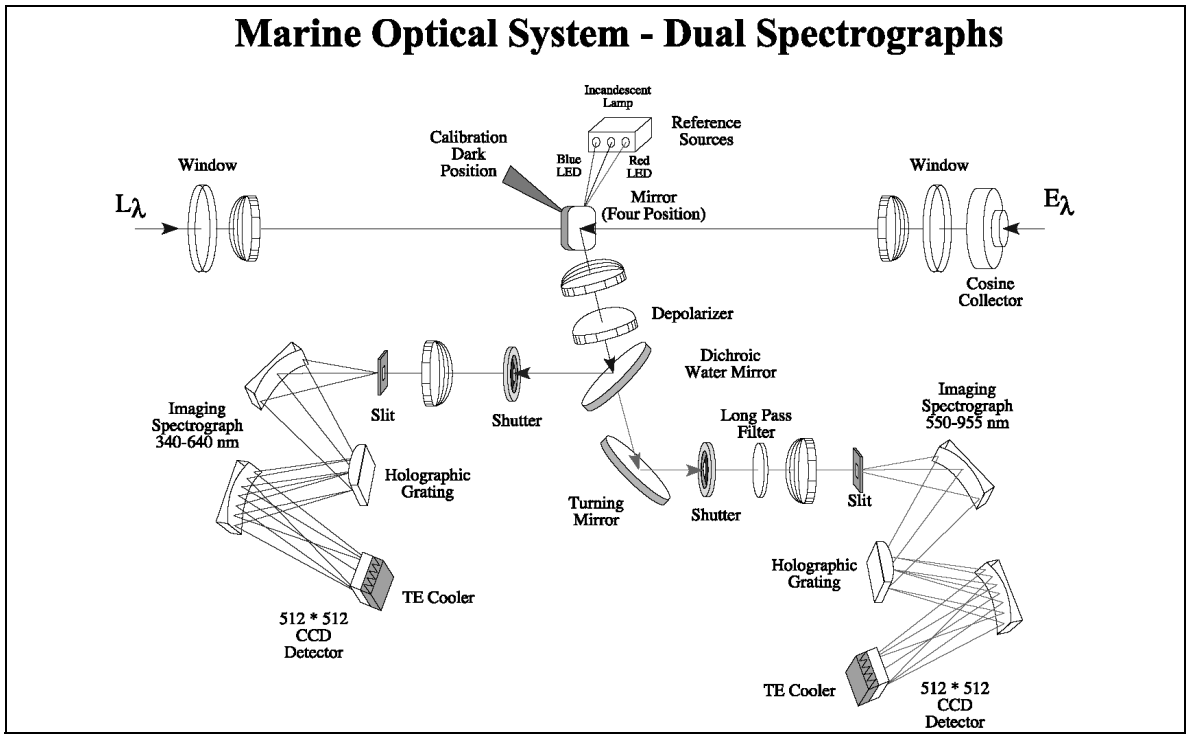

Figure 11.8: A schematic diagram showing the optical design of the MOS spectrographs.

Figure 11.9: Deployment of a MOBY.

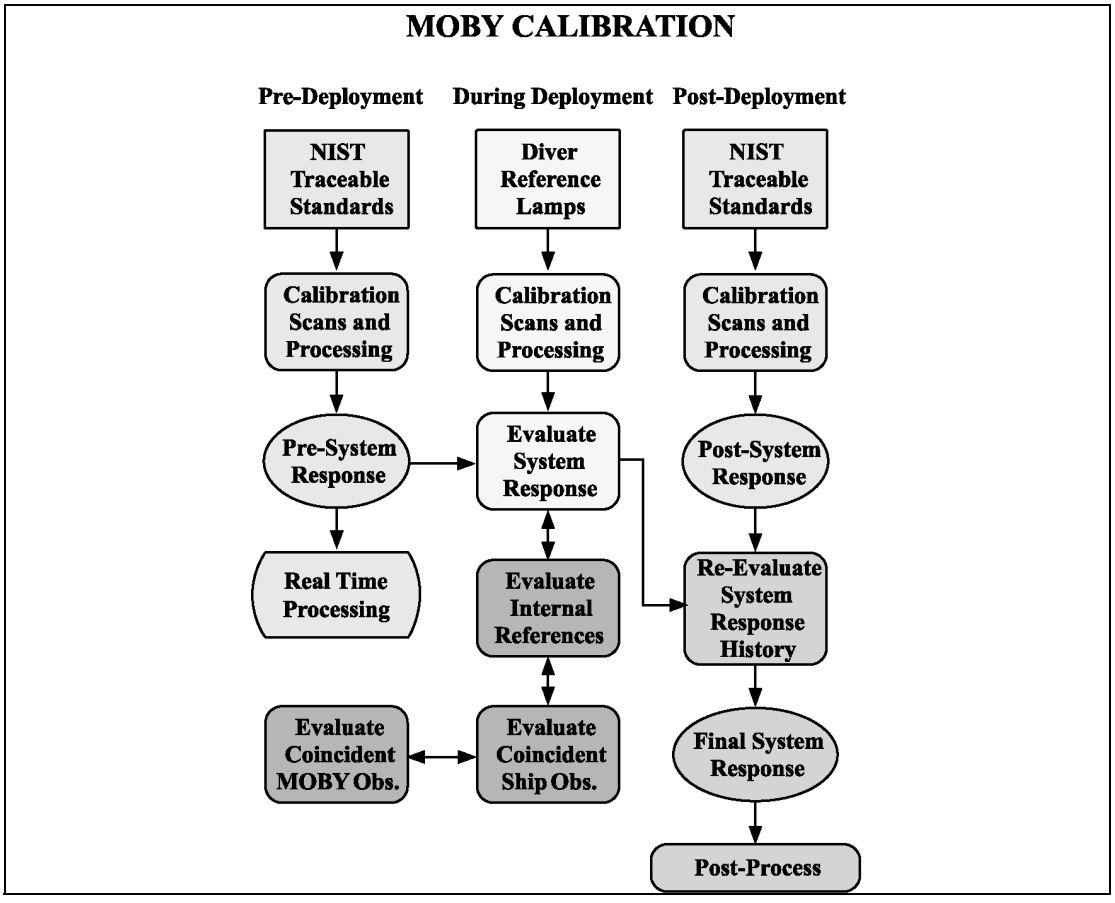

Figure 11.10: MOBY radiometric calibration and system stability check flow chart.

Figure 11.11: The diver-deployed underwater radiometric stability reference unit attached to an upwelling radiance collector on MOBY.

MOBY System Operations Scheduling

MOBY data collection is programmed at the MOBY Operations Site in Honolulu, prior to each deployment. After the buoy has been deployed, any necessary program changes are made using a direct connection to the buoy's on-board computer. The on-board computer is programmed to acquire data during each event when the mooring site is in view of a satellite ocean color sensor. Currently, the MOBY radiometric measurement sequence, described below, is executed twice daily, coincident with the predicted overpasses of SeaWiFS and MODIS.

Radiometric Measurements

The MOS measures radiation input from one $L_u(z,\lambda)$, $E_d(z,\lambda)$ or $E_s(\lambda)$ head at a time. The desired channel is selected by the optical multiplexer. A rotating mirror within the MOS selects alternatively the input from the multiplexer, a dark reference calibration, light emitting diodes (LEDs), or a tungsten halogen incandescent lamp (Table 11.3). Integration times for the radiance collector on the top arm, at 1 m, typically range from 1 s to 4 s for the blue spectrograph and 10 s to 30 s for the red spectrograph. A typical sequence would be to measure $L_u(\lambda,z)$ from a depth, preceded and followed by $E_s(\lambda)$ surface reference spectra and associated dark spectra. Then this sequence is repeated at the 2nd and 3rd depths to complete the profile for $L_u(\lambda,z)$, as summarized in the example of Table 11.6. Note that there are a total of 35 measurements for radiances at the 3 depths, surface irradiance $E_s(\lambda)$ and sensor dark spectra. The 35 measurements are grouped into overlapping subsets of 15 measurements, representing the cycle associated with upwelled radiance measurements at each depth. Not included in the example are measurements from the base of the MOS itself, because these data are not currently used to determine water-leaving radiance. This entire procedure requires between 30 min and 1 hr to complete.

Methods for Mitigating Bio-Fouling

Marine organisms, including algae and barnacles, typically attach themselves to any surface that is immersed in seawater for an extended period. This "bio-fouling" process changes the transmittance of the radiance windows and irradiance cosine diffusers. The radiance windows are placed at the base of copper tubes, and small amounts of bromide are slowly released near the windows throughout the deployment. Both of these substances are poisons for most marine life. It is not practical to use this approach with the irradiance collectors, so a combination of Teflon collector material, copper bezels and less effective anti-fouling compounds is used here. Divers clean the optical collectors and recharge the bromide dispensers at monthly intervals during each deployment.

Ancillary Measurements

Aboard the mooring buoy, the meteorological state variables (wind velocity, surface pressure, air temperature and humidity), sea surface temperature and conductivity, and near-surface *in situ* chlorophyll *a* fluorescence, are sampled as 5 min averages at 15 min intervals, and recorded continuously on the system disk. The data records are downloaded once daily.

Sun Photometer and Sky Radiance Measurements (on Lanai and Oahu)

The AERONET Project at NASA GSFC operates the CIMEL[1] sun photometers on Lanai and Oahu, and retrieves the data, remotely. The aerosol optical thickness and sky radiance distribution data measured at these sites are needed as input to atmospheric correction models when the MOBY water leaving radiances are used for vicarious calibration of the satellite ocean color sensor. The data are archived by, and may be obtained from, the AERONET Project at NASA GSFC. MOBY support personnel visit the photometer sites at monthly intervals to check and clean the instruments.

11.4 CALIBRATION AND QUALITY CONTROL

The MOBY radiometers are characterized and calibrated using procedures that conform to the protocols described in Chapter 6. The unique role of MOBY as a primary, long term, and daily reference for vicarious calibration of satellite ocean color sensors requires radiometric measurements of the highest possible quality, and this in turn places stringent demands on the methods of traceability to NIST radiometric standards. For example, the MOBY team uses exclusively irradiance standards acquired directly from NIST, NIST recalibrates these sources frequently (see below), and NIST investigators validate the team's radiometric sources at annual intervals.

The MOS radiometers are calibrated before and after each deployment, and stability tests are made during deployments using both on-board and diver-deployed sources. These calibrations, tests and comparative measurements are illustrated schematically in Figure 11.10. The special aspects of the MOBY radiometric calibration, characterization and stability test procedures are described in this section.

Radiometric Calibration and Characterization of MOS

The spectral irradiance responsivities of the MOS $E_d(z,\lambda)$ and $E_s(\lambda)$ channels are calibrated using FEL-type lamp standards of spectral irradiance, and the $L_u(z,\lambda)$ channels are calibrated using lamp-illuminated integrating sphere sources. The wavelength calibration is performed using spectral line emission lamps, and every calibration cycle includes a measure of three internal sources (see below). Each instrument, whether for a MOCE or for a MOBY deployment, is calibrated at the support facility site in Honolulu before and after the in-water deployment. The standards of spectral irradiance and radiance are recalibrated every 50 h of operation. The irradiance standards, 1000 W quartz-halogen lamps (model number FEL), are calibrated by NIST. The integrating sphere source radiance standards are calibrated by their manufacturer, Optronic Laboratories, Inc. The MOS irradiance responsivity assignments are NIST-traceable using the NIST-issued FEL lamps. During the MOS irradiance calibration, the lamps are operated at the correct current using a calibrated shunt resistor in series with the lamp. The lamp is operated in an enclosed

housing at the same distance and with the same collection area as at NIST (50 cm and 1 cm^2, respectively). A reference mounting plate ensures the alignment of the lamp to the irradiance collector. The validity of this approach was verified by NIST (Mueller *et al.* 1996).

The radiance assignment is NIST-traceable via the commercial standards laboratory's calibration of integrating sphere sources (ISSs). Two ISSs are used: model OL420 and model OL425. They are externally illuminated, with an aperture wheel to vary the radiant output in discrete amounts. However, the two ISS units differ in the designs of their internal baffles, and in the method used by each to continuously vary the output. The ISSs are operated at constant current. The OL425 has, additionally, an internal illuminance monitor detector that is used to relate the output to that during the calibration measurements at Optronic Laboratories. The ISSs are re-lamped by Optronic Laboratories, and calibrated before and after this procedure, so for each sphere and lamp configuration, there is an initial and a final radiometric calibration; to date, only the initial calibration values have been used for the MOBY calibrations.

In addition to the routine calibration of the MOBY radiometric standards, two single-channel, dual-mode radiometers were designed and built by NIST to verify the calibrations of the FELs and ISSs and to monitor their stability at the support facility site in Honolulu. These Standard Lamp Monitors (SLMs) (Clark *et al.* 2001) have interchangeable foreoptics for operation in either radiance or irradiance mode. The narrowband (approximately 10 nm bandwidth) interference filters are centered at 412 nm and 872 nm. During every radiometric calibration at the support site, the SLMs are used to record the output of the radiometric standards. The absolute radiometric response of the SLMs is determined by measurements at NIST, both during the initial development and subsequently on an interval of 12 months to 18 months.

Finally, site visits by NIST personnel are done at regular intervals, and radiance comparisons are performed. Initially, the SeaWiFS Transfer Radiometer (SXR), a multichannel filter radiometer (Johnson *et al.* 1998) that is calibrated at NIST, was used. At the present time, a later version of the SXR, the Visible Transfer Radiometer (VXR) (Johnson *et al.* 2002) is used, along with a stable, portable, NIST-calibrated ISS, the NIST Portable Radiance Source (NPR) (Brown and Johnson 2002). The VXR and the NPR were developed by NIST in support of the calibration program for the Earth Observing System (EOS) (Butler *et al.* 1999).

MOS Internal Reference Sources

An internal reference system was incorporated into the MOS design to monitor the stability of the radiometric detectors, electronics, and internal optics. These measurements are critical for establishing confidence in the observations acquired during a deployment cycle. One of the viewing positions on the main relay mirror mechanism reflects light from a Spectralon[1] diffuser plate into the blue and red spectrograph optical relays. The diffuser is illuminated in sequence by an incandescent lamp, a blue light emitting diode (LED), and a red LED. The blue and red diodes are centered at 465 nm and 705 nm, respectively, with approximately 100 nm bandwidths. The lamps are run with current controlled circuitry and the temperature of the lamp holder block is monitored. These lamps are observed at the end of each MOBY data acquisition set (Sect. 11.3). Time histories of reference lamp responses for each deployment period show the MOS spectrograph responses to be stable at the 1 % level.

Field Tests of Radiometric Stability Using Diver Deployed Sources

The internal reference lamp and diodes responses (above) do not reflect changes in the throughput of the MOS irradiance and radiance collectors due to bio-fouling. During the nominal three-month duration of a MOBY system deployment period, a team of divers conducts inspections, external reference lamp stability tests, and cleaning monthly. During these maintenance operations, the near-surface components of the moored buoy and MOBY are inspected for damage, deterioration, and bio-fouling. The condition of the buoy is documented with underwater photography. To document these effects on MOBY radiometry, external underwater reference lamp stability baseline measurements are conducted on each irradiance, or radiance, collector immediately after the MOBY is deployed (Fig. 11.11). The underwater reference lamp radiometric stability tests are repeated during each monthly service visit, before and after each collector is cleaned. The reference lamp system is a modified commercial underwater unit using a 35 W incandescent lamp. The lamp is powered by a submersible, 12 V, 6.5 A h battery-pack. Modifications to the

commercial lamp system included the addition of constant current circuitry to the battery pack, and construction of lamp housings that fit over the radiance and irradiance collectors to block ambient light, while maintaining a fixed distance between the lamp source and collector. The radiance reference lamp system has a translucent diffuser placed between the lamp and collector window. Laboratory stability tests of the reference lamp systems show the output to be repeatable within 1 % if the battery voltage remains within 25 % of full charge. In the field, batteries are replaced and recharged when voltage decreases to 50 % of full charge.

Examples of the diver reference lamp responses for a few wavelengths at one upwelling radiance collector are illustrated in Fig. 11.12. Data shown at each wavelength represent the difference between the MOS responses on 3 August 2000, when the MOBY was deployed, and the responses before and after cleaning on 4 October 2000. The vertical bars illustrate the standard uncertainty in the diver reference lamp comparisons. Because all the response measurements fall within this uncertainty, the diver lamp response data have not been used to correct for trends during a deployment.

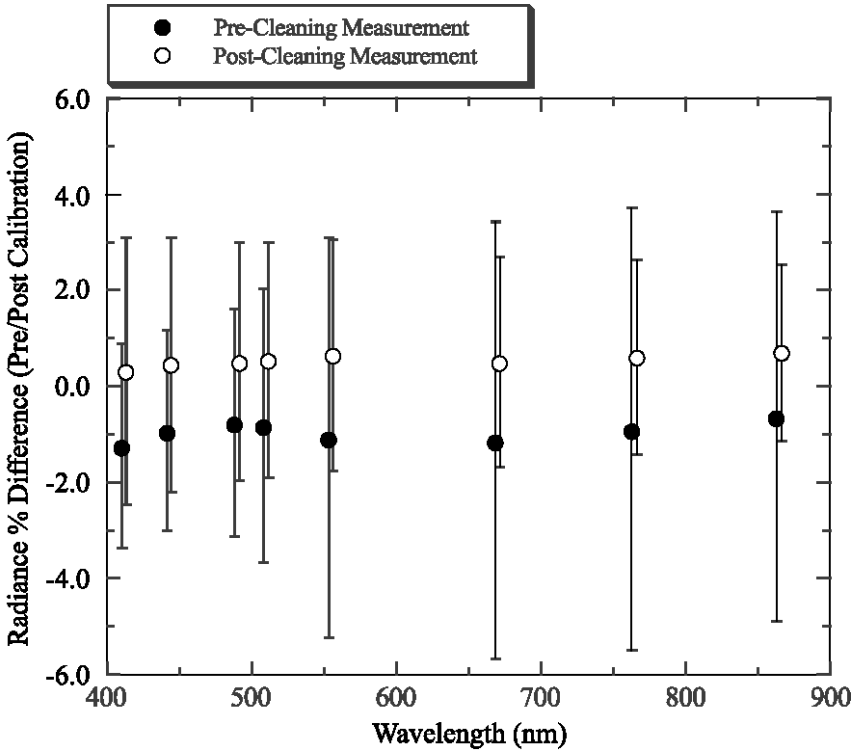

Figure 11.12: An example showing results of diver-deployed underwater radiometric stability source tests for several wavelengths and one radiance collector. The measurements were made immediately before, and after, the diver cleaned the radiance collector. The data are charted as percent differences from the similar test done on the day the buoy was deployed, approximately 2 months earlier.

Wavelength Stability Tests Using Fraunhofer Lines

Solar Fraunhofer lines and the atmosphere's oxygen A band absorption near 762 nm are resolved in the MOS $E_S(\lambda)$ spectra. The MOS detector array pixel locations of these lines are used to monitor the wavelength stability of the system throughout each deployment. Within the spectral resolution of the MOS spectrographs, no changes in the locations of any of these bands have occurred since the first MOBY deployment.

Stray Light Characterization

A critical issue in ocean color measurements arises because of the large difference in the relative spectral shape of the lamp-illuminated ISS (radiance mode), or the FEL lamp (irradiance mode), when compared to the relative spectral shape of $L_u(z,\lambda)$, or $E_d(z,\lambda)$, measured in the ocean. Radiometric sensors

do not have an ideal spectral selectivity, *i.e.*, the response at a wavelength of interest to flux at other wavelengths is small but finite (Chapter 5, Sect. 5.2 and Chapter 6, Sect. 6.4). As a result, measurements at the wavelength of interest include both a component that is proportional to the flux at that wavelength (*e.g.*, the "in-band" component) plus a component that sums the product of the sensor response and the spectrum of flux at wavelengths outside the in-band region. The latter sum, representing the out-of-band component, must be evaluated for all wavelengths for which the detector has finite responsivity. For MOS, the out-of-band response is largely determined by the scattering properties of the grating and unwanted reflections of flux diffracted in second order. We refer to the effect as "stray light".

Stray light considerations for MOS motivated dividing the spectrum into two regions using a dichroic beamsplitter and two spectrographs. As seen by the blue spectrograph, this division results in a better match between the spectral shapes of the FEL-type spectral irradiance sources and $E_d(z,\lambda)$, or the ISSs and $L_u(z,\lambda)$, and minimizes stray light effects in the critical ocean color wavelength bands. At 412 nm and 440 nm, for example, comparisons of $L_u(z,\lambda)$ for MOCE or MOBY deployments agree with measurements using independent filter radiometers to within ±5 %.

The effect of stray light in MOS is most evident in the region of overlap between the two spectrographs, from 545 nm to 650 nm. For the red spectrograph, the decreased transmittance of the dichroic beamsplitter in this region, where it goes from zero to nearly unity transmittance, means that the ratio of the in-band to the out-of-band components is unfavorable. Indeed, for some MOS wavelengths (CCD columns) at the blue side of the red spectrograph, the recorded signals can be dominated by the out-of-band component. At the present time, the processing algorithms use the results from the blue spectrograph up to 620 nm, and those from the red spectrograph beyond 620 nm. The differences are generally stable in time and depend on depth, another indication that the effect is related to source spectral shape.

To correct for stray light, the function that describes the sensitivity to flux at wavelengths other than the desired wavelength must be determined. This requires a tunable, monochromatic source that fills the entrance pupil of the sensor. Improvements in technology and the recent addition of new facilities at NIST have made it possible to fully characterize sensors such as CCD spectrographs using fully tunable laser-illuminated, integrating sphere sources (Brown, Eppeldauer, and Lykke 2000). The facility is called Spectral Irradiance and Radiance responsivity Calibrations with Uniform Sources (SIRCUS).

A thorough stray light characterization study for the MOBY project was begun in early 2000. Work started on SIRCUS with a MOS bench unit (Habauzit *et al.* 2002), and continued with the full characterization of MOS202 (which is used as a profiler instrument). Measurements are ongoing for the MOBY MOS units. The SIRCUS measurements yield the absolute radiance response of the sensors. Examples of the response of a single column in the blue spectrograph (column 380), and of the red spectrograph (column 277), are shown in Fig. 11.13 and Fig. 11.14 for the MOS profiler. The small peak near 510 nm for the blue spectrograph is caused by flux diffracted in second order and reflected onto the CCD by the grating and the second spherical mirror.

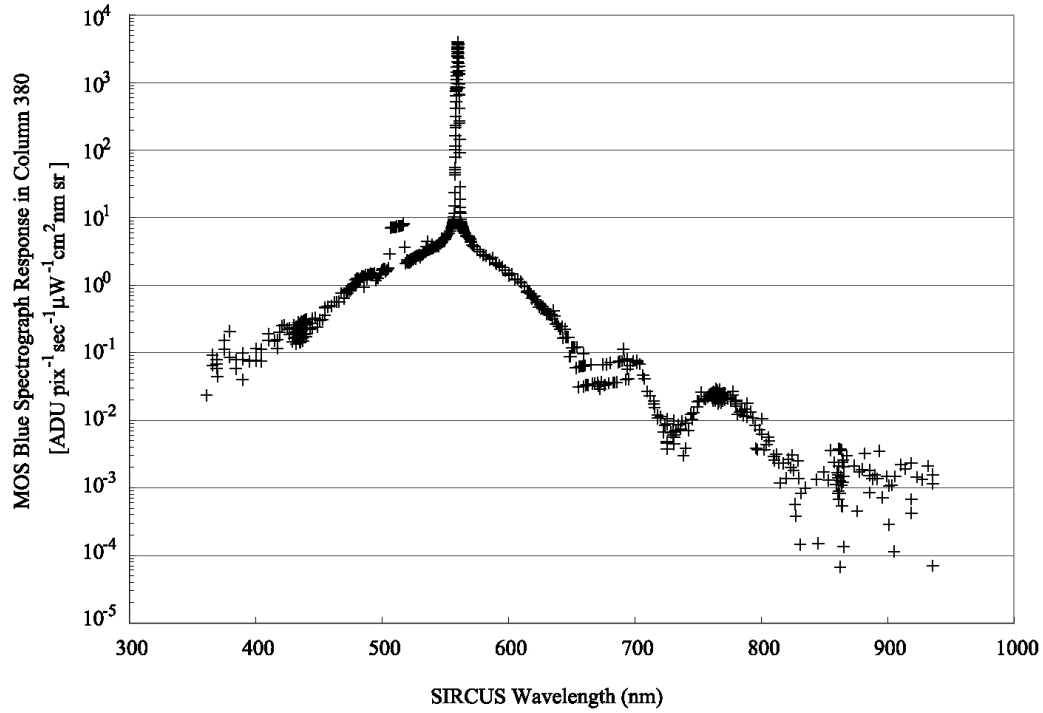

Figure 11.13: An example of the wavelength dependent spectral stray light responsivity of one CCD pixel location (wavelength) for the MOS blue spectrograph.

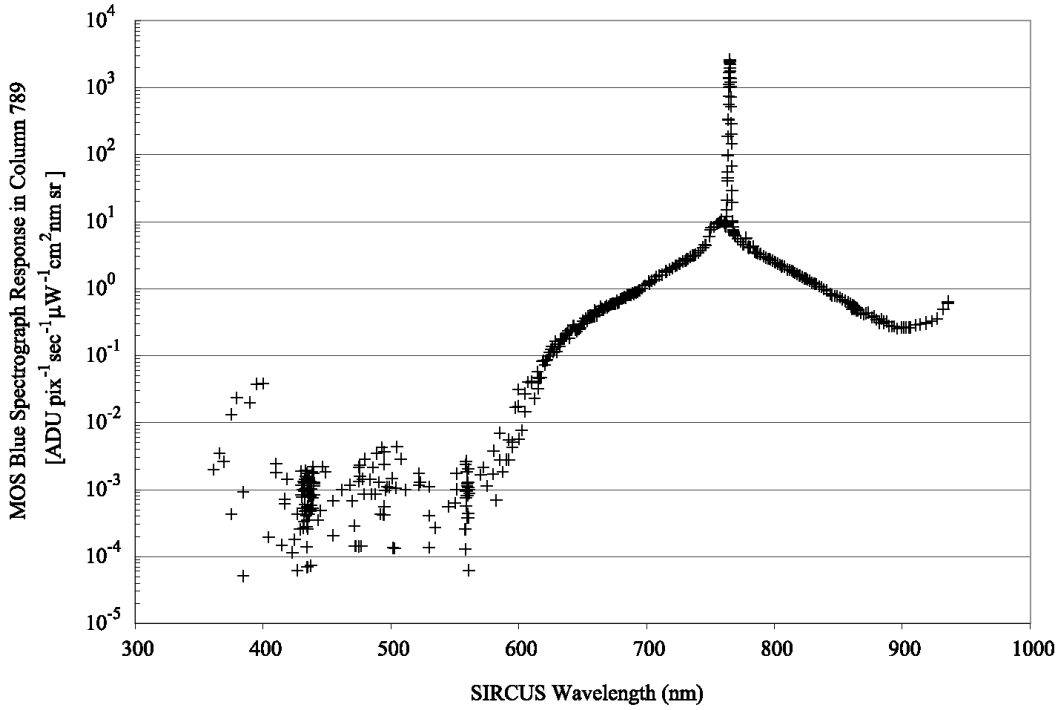

Figure 11.14: Same as Figure 11.13, but for one CCD pixel of the MOS red spectrograph.

A stray light correction algorithm was developed that is based on determination of the in-band region for one column on each CCD spectrograph, a description of the shape of the out-of-band response, and a model to account for the effects of the second order "reflection peak" (Brown *et al* 2002). To date, the SIRCUS results for the MOS profiler have been used to implement a preliminary version of the stray light correction algorithm, and test applications to the MOCE5 data sets are extremely encouraging. These preliminary results indicate that stray light affected the MOS Profiler results during MOCE 5 by up to +5 % at 412 nm (the uncorrected radiances are too small) and up to -1.5 % at 546 nm (the uncorrected radiances are too large).

Validation of the stray light correction algorithm is accomplished using an ISS that is made to simulate the spectral shape of in-water radiances using colored glass filters. The radiance of this colored source is determined independently by a NIST calibrated double grating monochromator. The results are compared to the corrected and uncorrected MOBY values and used to estimate the uncertainty of the stray-light correction.

CIMEL Sun Photometer and Sky Radiance Sensor Calibrations

The CIMEL instruments deployed at the stations on Oahu and Lanai are calibrated and maintained at NASA GSFC by the SIMBIOS Project Office, in collaboration with AERONET Project, following the procedures described in Chapter 7.

11.5 DATA ANALYSIS METHODS

As described above in Sect. 11.3, a single MOBY observation comprises a sequence of four to seven spectral radiance and irradiance measurement cycles for optical collectors located at the different depths on the spar (Table 11.6). The portion of the data record for an individual measurement cycle, *e.g.* for the upwelling radiance collector on a MOBY arm at depth z_i, is recorded as 3 arrays of digital counts $C_{Li}(\tau,N_p,z_i,t_m,\lambda)$ [m = 7, 8, 9 in an $L_u(z_i,\lambda)$ cycle of Table 11.6], where t_m is the time of the $m^{\underline{th}}$ measurement and τ is integration time. The "bin factor" N_p is expressed as the number of CCD rows read into the output register during each read step. Preceding and following each set of 3 radiance count arrays $C_{Li}(\tau,z_i,t_m,\lambda)$, the data record for one measurement cycle contains digital count arrays for incident surface irradiance (above water on the MOBY mast) $C_s(\tau_{sm},t_m,N_{pdm},\lambda)$, [m = 2, 3 4 (pre) and m = 12, 13, 14 (post) (Table 11.6)], and the MOS system dark response $D(\tau_{dm},t_m,N_{pdm},\lambda)$, for E_s [m = 1 and 5 (pre) and m = 11 and 15 (post)] and L_u [m = 6 and 10]. The central time, t_{Li} [or t_{Ei}], associated with a single radiance [or irradiance] measurement cycle (Table 11.6) is calculated as, *e.g.*

$$t_{Li} = \frac{1}{15}\sum_{i=1}^{15} t_i. \tag{11.1}$$

Temporal Averaging

The first step in processing the data is to scale each digital count array to unit integration time and average the individual measurements. Average counts for surface irradiance, normalized to unit integration time and bin factor, are computed as

$$\bar{C}_s\left(t_{Li},\lambda\right) = \frac{1}{6}\sum_m\left[\frac{C_s\left(\tau_{s,i},t_m,\lambda\right)}{N_{p,s,i}\tau_{s,i}}\right], m = 2,3,4,12,13,14 \text{ (Table 11.6)} \tag{11.2}$$

Average counts for MOS L_u Dark response, normalized to unit integration time and bin factor, are computed as (L_u cycle indices as in Table 11.6)

$$\bar{D}\left(t_{Li},\lambda\right) = \frac{1}{2}\left[\frac{D\left(\tau_{d,6},t_6,\lambda\right)}{N_{p,d,6}\tau_{d,6}} + \frac{D\left(\tau_{d,10},t_{10},\lambda\right)}{N_{p,d,10}\tau_{d,10}}\right]. \tag{11.3}$$

The 4 E_S Darks for the associated surface reference are averaged similarly. Finally, the average counts for the cycle of upwelled radiance measurements, normalized to unit integration time and bin factor, are computed as

$$\bar{C}_{\mathrm{L}i}\left(z_i,t_{\mathrm{L}i},\lambda\right)=\frac{1}{3N_{\mathrm{p}}\tau}\sum_{m=7}^{9}C_{\mathrm{L}i}\left(\tau,z_i,t_m,\lambda\right). \tag{11.4}$$

With appropriate changes in subscripts (*i.e.* "E*i*" in place of "L*i*"), equations (11.1) through (11.4) apply also to a spectral downwelling irradiance measurement cycle at depth z_i.

System Spectral Response Functions

The MOS system spectral radiance (or irradiance) responsivity functions $R_j(\lambda, \tau)$, for optical collector j and unit integration time (*i.e.* $\tau = 1$), are determined following procedures described in Chapter 6 (Sect. 6.2), with extensions described above in Sect. 11.4. Following the example cycle of M upwelling radiance scans for the MOBY arm at depth z_i, bracketed by surface irradiance and dark response records, incident spectral irradiances $E_S(t_{Li},\lambda)$ [μW cm^{-2}nm^{-1}] and average upwelling spectral radiance $L_u(z_i,t_{Li},\lambda)$ [μW cm^{-2}nm^{-1}sr^{-1}]

$$E_{\mathrm{s}}\left(t_{\mathrm{L}i},\lambda\right)=R_{\mathrm{Es}}\left(\lambda\right)\left[\bar{C}_s\left(t_{\mathrm{L}i},\lambda\right)-\bar{D}\left(t_{\mathrm{L}i},\lambda\right)\right], \tag{11.5}$$

and

$$L_{\mathrm{u}}\left(z_i,t_{\mathrm{L}i},\lambda\right)=R_{\mathrm{L}i}\left(\lambda\right)F_{\mathrm{imm}}^{\mathrm{L}i}\left(\lambda\right)\left[\bar{C}_{\mathrm{L}i}\left(z_i,t_{\mathrm{L}i},\lambda\right)-\bar{D}\left(t_{\mathrm{L}i},\lambda\right)\right], \tag{11.6}$$

where $F_{\mathrm{imm}}^{\mathrm{L}i}\left(\lambda\right)$ is the immersion factor for the i^{th} radiance collector as determined during the sensor's characterization (Chapter 6, Sect. 6.5 and Sect. 11.4). In equation (11.6), "L*i*" indicates that the subscripted (or superscripted) quantity applies to the spectral radiance collector mounted at depth z_i on the MOBY frame. Equation (11.6), substituting appropriate variables and subscripts, applies also to downwelling spectral irradiance $E_d(z_i,t_{Ei},\lambda)$ [μW cm^{-2}nm^{-1}] measurements using the irradiance collector mounted on MOBY at depth z_i.

Measurement Depths

On MOBY, $L_u(z,\lambda)$ is measured at 4 depths that are rigidly separated at fixed intervals on the buoy. These depths are nominally z_1 = 1 m, z_2 = 5 m, z_3 = 9 m, and z_4 = 11.5 m. The radiance measurement at 11.5 m is not currently used to determine water-leaving radiance. $E_d(z,\lambda)$ is measured only at nominal depths z_1, z_2, and z_3.

K(λ) Analysis

Following the above processing through equation (11.6), the attenuation coefficient for $L_u(z,\lambda)$ is computed from measurements at two discrete depths z_i and z_j as

$$K_{\mathrm{L}}\left(\bar{z}_{ij},\lambda\right)=\frac{1}{z_j-z_i}\ln\left(\frac{L_{\mathrm{u}}\left(z_i,\lambda\right)E_{\mathrm{s}}\left(t_j,\lambda\right)}{L_{\mathrm{u}}\left(z_j,\lambda\right)E_{\mathrm{s}}\left(t_i,\lambda\right)}\right),\ z_{\mathrm{j}}>z_{\mathrm{i}},\ i=1,2,3,\ j=2,3,4, \tag{11.7}$$

where t_i and t_j are the times of radiance measurements at depths z_i and z_j, respectively. The ratio of incident surface irradiances appears in (11.7) to account for changes in illumination, *e.g.* due to clouds, between the times of the two radiance measurements. The mean depth in the interval between z_i and z_j is

$$\overline{z}_{ij} = \frac{z_i + z_j}{2}. \tag{11.8}$$

The diffuse attenuation coefficient for $E_d(z,\lambda)$ is computed similarly to (11.7) as

$$K_d\left(\overline{z}_{ij},\lambda\right) = \frac{1}{z_j - z_i}\ln\left(\frac{E_d\left(z_i,\lambda\right)E_s\left(t_j,\lambda\right)}{E_d\left(z_j,\lambda\right)E_s\left(t_i,\lambda\right)}\right),\ z_j > z_i,\ i = 1,2,\ j = 2,3. \tag{11.9}$$

For computing $K_L\left(\overline{z}_{ij},\lambda\right)$ and $K_d\left(\overline{z}_{ij},\lambda\right)$ from data measured with the shipboard MOS instrument, the actual depths z_i are determined to the nearest cm using data from its high precision depth transducer.

Determining $L_W(\lambda)$ by Upward Extrapolation

To determine $L_W(\lambda)$, the measurement of upwelling radiance from a selected depth z_i is propagated to the surface as

$$L_u\left(0^-,\lambda\right) = L_u\left(z_i,\lambda\right)e^{K_L\left(\overline{z}_{ij},\lambda\right)z_i}. \tag{11.10}$$

The depth z_i is selected according to the following hierarchical rules:

1. If the data from the top arm are valid, then that depth is selected.
2. Else, the data from the middle arm, if valid, are selected.
3. Else, the data sequence is rejected entirely.

Water-leaving radiance is calculated by propagating $L_u(0^-,\lambda)$ through the interface as

$$L_W\left(\lambda\right) = \frac{1-\rho}{n^2}L_u\left(0^-,\lambda\right), \tag{11.11}$$

where the upward transmittance through the interface, for nadir viewing radiance, is approximately constant, with value

$$\frac{1-\rho}{n^2} = 0.543, \tag{11.12}$$

being only weakly dependent on wavelength and insensitive to wind speed (Austin 1974; see also Chapters 2, 10 and 13).

Normalized Water-Leaving Radiance

Since the water-leaving radiances are apparent optical properties and are dependent upon the effects of the atmosphere, variations in solar zenith angle θ_o, and the earth-sun distance *d*, it is necessary to normalize the data to remove these effects for some applications. The normalizing approach used with MOBY water-leaving radiances follows the procedures that were defined by Gordon and Clark (1981) to compute *solar-normalized water leaving radiances* as

$$L_{WN}\left(\lambda\right) = \frac{L_W\left(\lambda\right)}{t\left(\lambda,\theta_o\right)\cos\theta_o\left(\frac{d_o}{d}\right)^2}, \tag{11.13}$$

where d_o is the mean earth-sun distance, and $t(\lambda, \theta_o)$ is the diffuse atmospheric transmittance computed as

$$t\left(\lambda,\theta_o\right) = e^{-\frac{\frac{1}{2}\tau_R(\lambda)+\tau_{O_3}(\lambda)}{\cos\theta_o}}. \tag{11.14}$$

The Rayleigh optical thickness $\tau_R(\lambda)$ is taken for mean atmospheric pressure (Penndorf 1957), and the ozone optical thickness $\tau_{O_3}(\lambda)$ is computed for an atmospheric ozone concentration of 350 Dobson units. The ratio of average to actual earth sun distances is approximated as

$$\frac{d_o}{d} = 1 + 0.0167 \cos\left[\frac{2\pi(J-3)}{365}\right], \tag{11.15}$$

where J is the sequential day of the year.

The *normalized water-leaving radiances* $L_{WN}(\lambda)$ computed with Equations (11.13) through (11.15) are still dependent on the bidirectionality of the ocean's reflectance, as determined by the local inherent optical properties of the water and the solar zenith angle θ_o (Morel and Gentili 1996). To remove the bidirectional reflectance effects, it is necessary to convert the above $L_{WN}(\lambda)$ to *exact normalized water-leaving radiance* $L_{WN}^{ex}(\lambda)$ following the protocols in Chapter 13.

Spectral Band Averaging

The water leaving radiance corresponding to each wavelength band of a satellite ocean color sensor is determined from the MOBY solar-normalized water leaving radiances $L_{WN}(\lambda)$ as

$$L_{WN}^{MS}(\bar{\lambda}_i) = \frac{\int_0^\infty r_n^S(\lambda, \bar{\lambda}_i) L_{WN}(\lambda) d\lambda}{\int_0^\infty r_n^S(\lambda, \bar{\lambda}_i) d\lambda}, \tag{11.16}$$

where the superscripts S and MS denote a particular satellite ocean color sensor and a MOBY derived estimate for that satellite, respectively, $\bar{\lambda}_i$ is the effective wavelength of the i^{th} band of that sensor, and $r_n^S(\lambda, \bar{\lambda}_i)$ is the normalized relative spectral response function of that channel. In practice, (11.16) is approximated numerically.

An example MOBY water-leaving radiance spectrum is compared to the shapes of the spectral response function of MODIS ocean bands in Fig. 11.15. Note that $L_{WN}(\lambda)$ must be transformed to $L_{WN}^{ex}(\lambda)$ (Chapter 13) prior to match-up comparisons between MOBY and satellite water-leaving radiances.

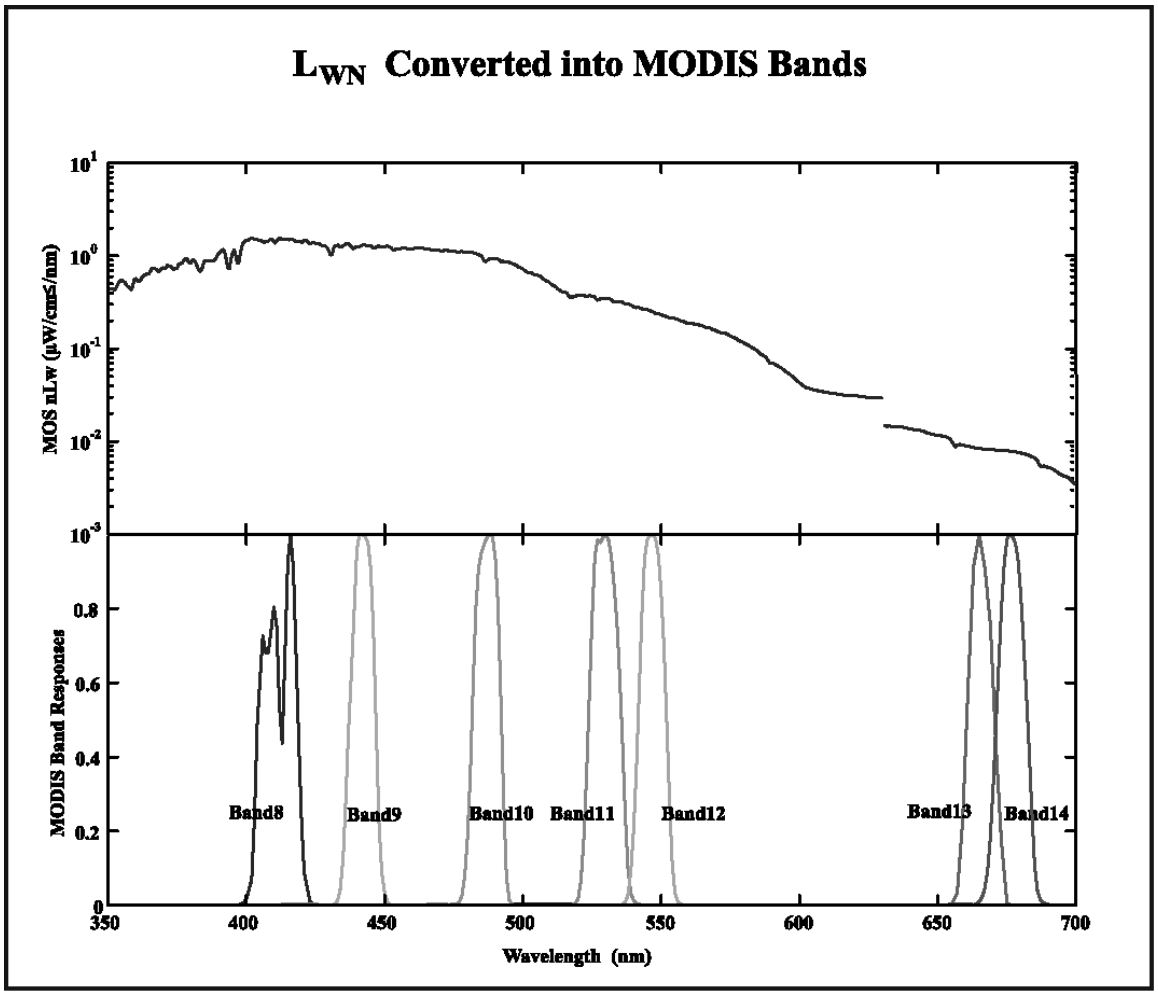

Figure 11.15: Comparison of a normalized water-leaving radiance spectrum measured by MOBY with the spectral band response functions of the MODIS ocean channels. The MOBY radiances have not been corrected for stray light, as is obvious from the large offset between the blue and red spectrographs at 630 nm.

11.6 DATA ARCHIVAL AND RECORDKEEPING

Band averaged water-leaving radiances for SeaWiFS and MODIS are transmitted to the SeaWiFS and SIMBIOS Project Offices, where they are archived in SeaBASS (Chapter 18). These data are also transmitted to and archived by the MODIS Team at the University of Miami. All data recorded by the MOBY system and on MOCE and other cruises are archived at MLML in Moss Landing, California and at NOAA NESDIS in Camp Springs, Maryland.

11.7 FUTURE DIRECTIONS

Temperature Characterizations

Although the MOS CCDs are temperature-controlled, the temperatures of the optical components in the spectrographs, the electronics, the MOBY fiber optics, and other system components are subject to environmental conditions. These ancillary instrument temperatures are recorded and archived, but are not used in the present data processing algorithms. Because the ambient temperature and degree of thermal equilibrium depends on the measurement purpose (calibration vs. in-water radiometry) and type of deployment (MOBY vs. MOS), the radiometric responsivities of MOBY and MOS are being studied as a

function of temperature. Various temperature-controlled baths are used, including one large enough for MOS.

Stray Light Characterizations

The MOBY Project includes a suite of instruments, requiring multiple field deployments to address the stray light issues. Once the required data are in hand, the stray light algorithm for all of the required instruments will be optimized. This may require separate model parameters for each input collector on MOBY. Then, the MOCE and MOBY data sets will be reprocessed, leading to an improvement in the accuracy of the derived $L_{WN}(\lambda)$'s that are used for vicarious calibration of MODIS, SeaWiFS, and other ocean color satellite sensors. It is anticipated that the uncertainty in the correction will be about 10 % of the effect, *e.g.* the uncertainty in the corrected values from stray light would be 0.5 % for a 5 % correction.

ACKNOWLEDGMENTS

The NIST efforts are supported by NOAA under contract NA00AANEG0072. Additional support for the NIST participation in this project has been provided under contracts S-41365-F (EOS Project Science Office) and S-64096-E (SeaWiFS Project). The Electro-optics Calibration Coordination Group, U.S. Air Force section, provided funding for SIRCUS (CCG98-439).

REFERENCES

Austin, R.W., 1974: The remote sensing of spectral radiance from below the ocean surface. In: Optical Aspects of Oceanography, N.G. Jerlov and E.S. Nielson, Eds., pp 317-344.

Brown, S.W., G.P. Eppeldauer, and K.R. Lykke, 2000: NIST facility for spectral irradiance and radiance responsivity calibrations with uniform sources. *Metrologia*, **37**, 579-582.

Brown, S.W., and B.C. Johnson, 2002: Development of a portable integrating sphere source for the Earth Observing System's Calibration Validation Program. To appear in *International Journal of Remote Sensing*.

Brown, S.W., C. Habauzit, B.C. Johnson, and K.R. Lykke, 2002: Tunable-laser based calibration of a CCD spectrograph. In preparation.

Butler, et al. 1999: J.J. Butler J.J., B.L. Markham, B.C. Johnson, S.W. Brown, H.W. Yoon, R.A.Barnes, S.F. Biggar, E.F. Zalewski, P.R. Spyak, F. Sakuma, and J.W. Cooper, 1999: Radiometric measurement comparisons using transfer radiometers in support of the calibration of NASA's Earth Observing System (EOS) Snesors, in Sensors, Systems, and Next Generation Satellites III, Proc. SPIE Vol. 3870, Ed. P.L. Slater, (Bellingham, Washington: Society of Photo-Optical Instrumentation Engineers), 180-192.

Clark, D.K, H.R. Gordon, K.J. Voss, Y. Ge, W. Broenkow, and C.C. Trees, 1997: Validation of atmospheric corrections over oceans. *J. Geophs. Res*., **102**: 17209-17217.

Clark, D.K., M.E. Feinholz, M.A. Yarbrough, B.C. Johnson, S. W. Brown, Y.-S. Kim, and R.A. Barnes, 2001: Overview of the radiometric calibration of MOBY. *Proc. SPIE, Earth Observing Systems VI*, **4483**, xxx—yyy.

Clark, D.K, H.R. Gordon, K.J. Voss, Y. Ge, W. Broenkow, and C.C. Trees, 1997: Validation of atmospheric corrections over oceans. *J. Geophs. Res*., **102**: 17209-17217.

Evans, R.H. and H.R. Gordon, 1994: Coastal Zone Color Scanner system calibration: a retrospective examination. *J. Geophys. Res.*, **99**:7293-7307.

Fargion, G.S. and J.L. Mueller, 2000: *Ocean Optics Protocols for Satellite Ocean Color Sensor Validation, Revision 2*, NASA TM 2001-209955, NASA Goddard Space Flight Center, Greenbelt, Maryland, 184 pp.

Gordon, H.R., 1981: Reduction of error introduced in the processing of Coastal Zone Color Scanner-type imagery resulting from sensor calibration and solar irradiance uncertainty. *Appl. Opt.*, **20**: 207-210.

Gordon, H.R., 1987: Calibration requirements and methodology for remote sensors viewing the ocean in the visible. *Remote Sens. Environ*., **22**:103-126.

Gordon, H.R., 1988: Ocean color remote sensing systems: radiometric requirements. *Recent Advances in Sensors, Radiometry, and Data Processing for Remote Sensing*, P.N. Slater, Ed., SPIE, **924**: 151-157.

Gordon, H.R., J.W. Brown, O.B. Brown, R.H. Evans, and D.K. Clark, 1983: Nimbus-7 CZCS: reduction of its radiometric sensitivity with time. *Appl. Opt*., **24**:3929-3931.

Gordon, H.R. and D.K. Clark, 1981: Clear water radiances for atmospheric correction of Coastal Zone Color Scanner imagery. *Appl. Opt.*, **20:** 4174-4180.

Gordon, H.R., D.K. Clark, J.W. Brown, O.B. Brown, R.H. Evans, and W.W. Broenkow, 1983: Phytoplankton pigment concentrations in the middle Atlantic bight: comparison of ship determinations and CZCS estimates. *Appl. Opt*. **22:** 20-36.

Gordon, H.R. and K. Ding, 1992: Self shading of in-water optical instruments. *Limnol. Oceanogr*., **37**: 491-500.

Hooker, S.B. and S. Maritorena, 2000: An evaluation of oceanographic radiometers and deployment methodologies. *J. Atmos. Oceanic Technol*. **17**: 811-830.

Habauzit, C., S.W. Brown, K.R. Lykke, B.C. Johnson, M.E. Feinholz, M.A. Yarbrough, and D.K. Clark, 2002: Radiometric characterization and absolute calibration of the Marine Optical System (MOS) bench unit. Submitted to the Journal of Atmospheric and Oceanic Technology.

Johnson, B.C., J.B. Fowler, and C.L. Cromer, 1998: The SeaWiFS Transfer Radiometer (SXR). *NASA Tech. Memo. 1998-206892, Vol. 1*, S.B. Hooker and E.R. Firestone, Eds., NASA Goddard Space Flight Center, Greenbelt, Maryland, 58 pp.

Johnson, B.C., S.W. Brown, G.P. Eppeldauer, and K.R. Lykke, 2002: System-level calibration of a transfer radiometer used to validate EOS radiance scales. To appear in International Journal of Remote Sensing.

Morel, A. and B. Gentili, 1996: Diffuse reflectance of oceanic waters. III. Implication of bidirectionality for the remote-sensing problem. *Applied Optics*, **35**: 4850-4862.

Mueller, J.L. and R.W. Austin, 1992: Ocean Optics Protocols for SeaWiFS Validation. *NASA Tech. Memo. 104566, Vol. 5*, S.B. Hooker and E.R. Firestone, Eds., NASA Goddard Space flight center, Greenbelt, Maryland, 45 pp.

Mueller, J.L. and R.W. Austin, 1995: Ocean Optics Protocols for SeaWiFS Validation, Revision 1. *NASA Tech. Memo. 104566, Vol. **25***, S.B. Hooker and E.R. Firestone, Eds., NASA Goddard Space flight center, Greenbelt, Maryland, 66 pp.

Mueller, J.L., B.C. Johnson, C.L. Cromer, S.B. Hooker, J.T. McLean, and S.F. Biggar, 1996: The Third SeaWiFS Intercalibration Round-Robin Experiment, SIRREX-3, September 1994. *NASA Tech. Memo 104566, Vol. 34*, S. B. Hooker, E. R. Firestone, and J. G. Acker, Eds., NASA Goddard Space Flight Center, Greenbelt, Maryland, 78 pp.

Penndorf R., 1957: Tables of the refractive index for standard air and the Rayleigh scattering coefficient for the spectral region between 0.2 and 20.0 microns and their application to atmospheric optics, *J. Opt. Soc. Am.*, **47**, 176-182.

Siegel, D.A., M.C. O'Brien, J.C. Sorenson, D.A. Konnoff, E.A. Brody, J.L. Mueller, C.O. Davis, W.J. Rhea, and S.B. Hooker, 1995: Results of the SeaWiFS Data Analysis Round Robin, July 1994 (DARR-94). *NASA Tech Memo. 104566, Vol. **26***, S.B. Hooker and E.R. Firestone, Eds., NASA Goddard Space Flight Center, Greenbelt, Maryland, 58p.

Taylor, B.N., and C.E. Kuyatt, 1994: Guidelines for Evaluating and Expressing the Uncertainty of NIST Measurement Results. *NIST Tech. Note 1297*, U.S. Department of Commerce, National Institute of Standards and Technology, Washington, DC, 20 pp.

Table 11.1: Summary of MOCE data collection cruises. Cruises dedicated to the collection of bio-optical data are indicated with "MOCE". Cruises where data were collected in conjunction with MOBY operations are indicated with "MOBY".

Cruise	Cruise Dates	Cruise Location	No. of Stns	Satellite(s) Supported
MOCE-1	28 Aug-11 Sep 1992	Monterey Bay	7	
MOCE-2	27 Mar-14 Apr 1993	Gulf of California	13	
MOCE-3	27 Oct-15 Nov 1994	Hawaiian Archipelago	16	
MOBY-L14	14-22 Sep 1996	Hawaii-Lanai	6	
MOBY-L15	14-22 Nov 1996	Hawaii-Lanai	5	OCTS Initialization
MOBY-L16	23 -28 Feb 1997	Hawaii-Lanai	8	OCTS Initialization
MOBY-L20	19-27 Jul 1997	Hawaii-Lanai	5	
MOBY-L22	22 Sep-4 Oct 1997	Hawaii-Lanai	7	
MOBY-L25	7-15 Dec 1997	Hawaii-Lanai	3	
MOCE-4	26 Jan-12 Feb 1998	Hawaiian Islands	17	SeaWiFS Initialization
MOBY-L28	30 Mar-1 Apr 1998	Hawaii-Lanai	2	
MOBY-L35	23-26 Jul 1998	Hawaii-Lanai	5	
MOBY-L38	25-30 Oct 1998	Hawaii-Lanai	5	
MOBY-L43	6-11 Feb 1999	Hawaii-Lanai	3	
MOBY-L45	1-6 May 1999	Hawaii-Lanai	4	
MOCE-5	1-21 Oct 1999	Gulf of California	20	
MOBY-L54	10-15 Feb 2000	Hawaii-Lanai	2	
MOCE-6	9-16 Apr 2000	Hawaiian Islands	8	MODIS Initialization-Side A
MOBY-L56	15-19 May 2000	Hawaii-Lanai	3	
MOBY-L59	24 Jul-11 Aug 2000	Hawaii-Lanai	3	MODIS Initialization-Side A
MOCE-7	3-10 Dec 2000	Hawaiian Islands	7	MODIS Initialization-Side B
MOCE-8	28 Feb-9 Mar 2001	Hawaiian Islands	9	MODIS Initialization-Side B
MOBY-L69	1-4 Jun 2001	Hawaiian Islands	2	

Table 11.2a: MOBY Specifications	
Physical Specifications:	
Dimensions D x L (m)	1.7 x 15
Collector standoff length (m)	3.0 max
Weight in air (kg)	955
Height above waterline (m)	3
Reserve buoyancy (kg)	816
Flotation material	Isomer foam
Undamped period (sec)	2.5
Damping	Suspended drag device
Surface float frame	Welded stainless steel (T316L)

Spar	Stainless steel reinforced fiberglass		
Instrument Bay	Welded stainless steel (T316L)		
Collector standoff depths	Variable		
Optical:			
Spectrograph	MOS		
MOS optical interface	Fiber optic multiplexer, 10 ports		
Fiber optics	1mm silica/silica		
Fiber optic Interface	O-ring sealed SMAS		
Collectors:			
	E_s:	**E_d:**	**L_u:**
Dimensions	5 cm x 18 cm	5 cm x 17 cm	5 cm x 17 cm
Collector dimensions	3 cm	7 cm	2.8 cm
FOV	Cosine response	Cosine response	Max 5 °
f#	-	-	2
Electrical:			
Power source	4 x 40 W solar panels		
Charge control	Trace C12		
Battery monitoring	Individual monitor and charge control		
Average daily power production (W)	640		
Reserve battery capacity (W)	9600		
Instrument Bay battery type	4 x 200 A h, 12 v, Sealed Marine Gel Cell		
GPS	Raytheon RS112LP		
Argos	Seimac GPSMML		
R.F. beacon/locator strobe	Novatec, RF700C5		
Cellular antenna	Cellwave		
Controller battery type	80 A h, 12 v Sealed Marine Gel Cell		
Controller battery capacity	960		
Buoy power consumption, Sleep (uW)	3		
Buoy power consumption, Active (W)	9.6		
Buoy power consumption, Telemetry mode(W)	42		
Buoy power consumption, Acquisition mode (W)	132		
Surface Buoy Controller:			
Processor	MC68332		
Operating system	MLML Forth		
Modem	Zyxel, U-1496P		
Cellular transceiver	Motorola, S1765A		
Host serial interface	RS232, 9600 baud		
MOS serial interface	RS485, 9600 baud		
Subsurface power controller serial interface	RS485, 19.2k baud		
GPS serial interface	RS232, 4800 baud		
Internal power control	Latching relays		
A/D System:	**High resolution**	**Low resolution**	
Resolution	16 bit	12 bit	
Gains	1,10,100,500		
Channels	16	4	
Throughput	33 kHz, max	>100 kHz	
Accuracy	0.0024%, max	0.01%	
Subsurface Instrument bay Power Controller			
Operating system	TTBasic		
Status functions	Instrument bay power monitor		
	MOS power monitor		
	Battery charge monitor		
Control functions	Battery charge control		
	MOS power control		

Table 11.2b: MOBY Ancillary measurements

Parameter	Sensor Type	Range	Precision	Accuracy
Surface controller battery voltage (V)	Voltage monitor	0-25	0.006	0.02
Humidity	Monolithic capacitive	0-100 %	0.01%	2%
Case internal temperature (°C)	Thermistor	-10-50	0.05	0.1
Upper arm pressure (depth)	Strain gauge	0-25 meters	1.0 mm	5mm
Controller current (A)	Shunt	0-25	0.04	0.25
Controller battery charge current (A)	Shunt	0-25	0.04	0.25
Solar panel 1 current (A)	Shunt	0-25	0.04	0.25
Solar panel 2 current (A)	Shunt	0-25	0.04	0.25
Solar panel 3 current (A)	Shunt	0-25	0.04	0.25
Solar panel 4 current (A)	Shunt	0-25	0.04	0.25
Subsurface power controller voltage (V)	Voltage monitor	0-25	0.006	0.02
MOS voltage	Voltage monitor	0-25	0.006	0.02
MOS Battery current (A)	Shunt	0-25	0.04	0.25
MOS Battery #1	Voltage monitor	0-25	0.006	0.02
MOS Battery #2	Voltage monitor	0-25	0.006	0.02
MOS Battery #3	Voltage monitor	0-25	0.006	0.02
MOS Battery #4	Voltage monitor	0-25	0.006	0.02

Table 11.3a: MOS Spectrograph Characteristics

Dimensions:	
MOS only, D x L, (mm)	330 x 660
Weight in air (Kg)	64
Weight in sea water (Kg)	4
MOS with profiling rack and battery, D x L, (mm)	673 x787
Weight in air (Kg)	143
Weight in sea water (Kg)	122
Construction	O-ring sealed aluminum
Depth rating (meters)	100
Electrical:	
Profiler Lead-acid battery capacity (W)	600
MOS Power consumption (W)	120 W @ 10.5 – 14.5
Optics:	
Material (windows, lenses)	Fused Silica
Input optics f#	2
Diameter (mm)	43
FOV (deg)	Max 5 °
Input telescope ports	2 (up & down)
Polarization filter (option)	Quartz wedges
Input selection	4 positions
Input mirror settings	Up, Down, Reference, Dark
Spectrographs	2
Spectral separation optics	45° dichroic mirror
Separation wavelength, 50% pass (nm)	635
Full spectral range (nm)	340-955

Spectral resolution (nm)	<1
Polarization sensitivity	<1% (with depolarizing optics option)

Spectrographs:	
Dimensions, L x W x H (mm)	178 x 152 x 100
Type	Offner variant
Construction	Stainless steel (T316) bench Aluminum fixtures
Optics	SiO protected, Al coated glass (Blue) Au coated, black glass (Red)
Grating	Convex holographic
Wavelength Range (nm)	340 - 640 (Blue) 550 - 955 (Red)
Focal length (mm)	100
f#	3.8
Slit dimension (um)	12 (h) * 25 (w) * 40 (t)
Slit material	Electroformed Nickel
Resolution (nm)	0.6 (Blue) / 0.8 (Red)
Bandpass, FWHM, over spectrograph range, (nm)	1.0 - 1.2 (Blue) / 1.28 - 1.5 (red)
Fore optics	Ø25 mm, Cylindrical
Out of band rejection filters	580 nm High Pass (Red)

Table 11.3b: MOS Ancillary Measurements

Parameter	**Sensor Type**	**Range**	**Precision**	**Accuracy**
Mains (Battery) voltage	Voltage monitor	0-25 V	0.006 V	0.02 V
Humidity	Monolithic capacitive	0-100 %	0.01%	2%
Case internal temperature	Thermistor	-10-50°C	0.05	0.1
Water Temperature	Thermistor	-10 to 50 °C	0.005	0.05
Pressure (depth)	Strain gauge	0-200 meters	1.0 cm	4.0 cm
Tilt-X	Electrolytic	±60°	0.0026 °	0.03 °
Tilt-Y	Electrolytic	±60°	0.0026 °	0.03 °
Blue Array Temperature	Thermistor	-50 to 40°C	0.005 °C	0.05 °C
Red Array Temperature	Thermistor	-50 to 40°C	0.005 °C	0.05 °C
Blue Calib diode monitor	Photodiode	NA	15-bit	0.001%
Red Calib diode monitor	Photodiode	NA	15-bit	0.001%
Calib. Source block temp	Thermistor	-10 to 50 °C	0.005	0.05 °C
Coolant Flow	Pelton Wheel	20-2000 ml/min	1.5 ml/min	0.01 ml/min
Depth Sensor Temperature	Thermistor	-10 to 50 °C	0.005	0.05 °C
System Current	Hall effect	0 - 20 A	.01 A	0.05 A
Blue CCD Heater Monitor	Voltage monitor	NA	15-bit	0.001%
Red CCD Heater Monitor	Voltage monitor	NA	15-bit	0.001%
Internal Temperature at TT7	Thermistor	-10-50°C	0.05	0.1
Blue CCD Head Temperature	Thermistor	-10 to 50 °C	0.005	0.05 °C
Red CCD Head Temperature	Thermistor	-10 to 50 °C	0.005	0.05 °C
Heading	Flux gate compass	0 to 360 °	0.1°	0.5 °

Table 11.4: Summary of MOBY Deployment and Interim Servicing Cruises.

Cruise Name	Cruise Dates	Mooring	Diver Cals	MOBY	CIMEL
MOBY-L1	3-7 Oct 93	deployed			
MOBY-L2	6-10 Feb 94			aborted deploy	
MOBY-L3	21-25 Feb 94			deployed	
MOBY-L4	24-29 Mar 94		X		
MOBY-L5	5-9 May 94			check-up	
MOBY-L6	24-27 May 94		cancelled-bad weather		
MOBY-L7	25-30 Jun 94	retrieved		recovered	
MOBY-L8	9-12 Sep 94			testing	
MOBY-L9	8-27 Mar 95			testing	
MOBY-L10	15-30 Aug 95			testing	
MOBY-L11	3-8 Nov 95	deployed			
MOBY-L12	21 Feb-6 Mar 96			testing	
MOBY-L13	24 Jul-15 Aug 96			testing	X
MOBY-L14	14-21 Sep 96			deployed	
MOBY-L15	2-4, 14-22 Nov 96			exchanged	
MOBY-L16	23 Feb-2 Mar 97			recovered	
MOBY-L17	1-17 Apr 97			assembly	
MOBY-L18	9-23 May 97			testing	
MOBY-L19	9-23 Jun 97			testing	
MOBY-L20	19-27 Jul 97			deployed	
MOBY-L21	31-Aug-97		X		
MOBY-L22	22 Sep-4 Oct 97		X		
MOBY-L23	30-31 Oct 97			retrieved/reattached	
MOBY-L24	10-11 Nov 97		X		
MOBY-L25	7-14 Dec 97	exchanged	X	exchanged	
MOBY-L26	13-14 Jan 98		X		
MOBY-L27	9-10 Mar 98		X		
MOBY-L28	29 Mar-2 Apr 98			aborted-bad weather	
MOBY-L29	21-24 Apr 98			exchanged	X
MOBY-L30	4-May-98		cancelled-bad weather		X
MOBY-L31	15-May-98			maintenance	X
MOBY-L32	2-3 Jun 98		X		
MOBY-L33	21-Jun-98			repair	X
MOBY-L34	2-3 Jul 98		X		X
MOBY-L35	22-26 Jul 98			exchanged	

MOBY-L36	25, 28-29 Aug 98		cancelled-bad weather		X
MOBY-L37	17, 19-20 Sep 98		X	maintenance	
MOBY-L38	24-30 Oct 98		X	exchanged	X
MOBY-L39	7-10 Dec 98		X	maintenance	
MOBY-L40	5-Jan-99			maintenance	
MOBY-L41	10-12 Jan 99		X		X
MOBY-L42	21-Jan-99			maintenance	
MOBY-L43	6-11 Feb 99	exchanged	X	exchanged	
MOBY-L44	9-11 Mar 99		X	maintenance	X
MOBY-L45	1-6 May 99		X	exchanged	
MOBY-L46	2-3 Jun 99		X	maintenance	X
MOBY-L47	29 Jun-1 Jul 99		X	maintenance	X
MOBY-L48	29 Jul-1 Aug 99		X	exchanged	
MOBY-L49	5-Sep-99			check-up	
MOBY-L50	10-Oct-99			check-up	
MOBY-L51	15-18 Nov 99		X	exchanged	
MOBY-L52	16-19 Dec 99		X		X
MOBY-L53	25-Jan-00			maintenance	X
MOBY-L54	10-15 Feb 00	exchanged	X	exchanged	
MOBY-L55	29-31 Mar 00		X	maintenance	
MOBY-L56	15-19 May 00		X	exchanged	
MOBY-L57	19 -21 Jun 00		X		X
MOBY-L58	17-19 Jul 00		X		
MOBY-L59	3-6 Aug 00		X	exchanged	
MOBY-L60	12-14 Sep 00		X		X
MOBY-L61	23-Sep-00			maintenance	
MOBY-L62	5-6 Oct 00		X		X
MOBY-L63	9-11 Jan 01		X		X
MOBY-L64	28-Jan-01			maintenance	
MOBY-L65	7-8 Feb 01		X		
MOBY-L66	18-Mar-01			check-up	
MOBY-L67	7-9 Apr 01		X		X
MOBY-L68	22-23 May 01			maintenance	X
MOBY-L69	1-4 Jun 01		X	exchanged	
MOBY-L70	4-6 Jul 01		X	maintenance	X

Table 11.5: *In situ* observations collected during a MOCE cruise in support of vicarious calibration/validation of satellite ocean color systems. Measurement subcategories follow those shown in Chapter 3, Table 3.1.

MOCE Cruise Data Acquisition	Institution	Instrumentation System
Required Measurements		
Downwelled Irradiance	MLML	MOS, SPMR
Upwelled Radiance	MLML	MOS, SPMR
Incident Irradiance	MLML	SIS, SMSR
Aerosol Optical Depth	NOAA/NESDIS, U of Miami	HHCRM, MicroTops
Phytoplankton Pigment Composition	CHORS	HPLC
Chlorophyll a and Phaeopigment Concentration	CHORS	Fluorometric
Latitude and Longitude	NOAA/NESDIS	Trimble GPS
Date and Time (UTC)	NOAA/NESDIS	Trak
Wind Speed and Direction	NOAA/NESDIS	Young
Surface Barometric Pressure	NOAA/NESDIS	Setra
Air Temperature/Relative Humidity	NOAA/NESDIS	Vaisala
Cloud Cover	NOAA/NESDIS	Sky Camera
Secchi Depth	MLML	Secchi Disk
Highly Desired Measurements		
Beam Attenuation	NOAA/NESDIS	VLST
Beam Attenuation Profiles	MLML	WETLabs C-Star
Particle Absorption	NOAA/NESDIS	Diode Array Spectrophotometer
Dissolved Material (CDOM) Absorption	NOAA/NESDIS	Diode Array Spectrophotometer
Non-Pigmented Particle Absorption	NOAA/NESDIS	Diode Array Spectrophotometer
Phytoplankton Absorption	NOAA/NESDIS	Diode Array Spectrophotometer
Fluorometric Profiles	MLML	Chelsea
Whitecap Conditions	U of Miami	
Conductivity and Temperature Profiles	MLML	SeaBird CTD
Conductivity and Temperature - Alongtrack	NOAA/NESDIS	Falmouth TSG
Specialized Measurements		
Instrument Self-Shading	NOAA/NESDIS	FOS
Upwelled Radiance Distribution	U of Miami	RADS
Particle Size Data	NOAA/NESDIS	Laser Particle Counter
Total Suspended Particulate Matter (TSM)	MLML	
Particulate Organic Carbon/Nitrogen (POC/PON)	MLML	

Table 11.6: An example of a MOBY MOS upwelled radiance measurement cycle. The cumulative index is the order in which measurements are made. The $L_u(z_i,\lambda)$ Cycle Indices group the measurements at depth z_i with bracketing $E_s(\lambda)$ measurements and associated dark measurements; these indices are used in Equations (11.1) through (11.4) to average the individual measurements within each cycle.

Cumulative Index	**Variable Measured**	**Depth z (m)**	$L_u(z_1,\lambda)$ **Cycle Index**	$L_u(z_2,\lambda)$ **Cycle Index**	$L_u(z_3,\lambda)$ **Cycle Index**
1	$E_s(\lambda)$ Dark	--		1	
2 – 4	$E_s(\lambda)$	0^+		2 – 4	
5	$E_s(\lambda)$ Dark	--		5	
6	$L_u(\lambda)$ Dark	--		6	
7 – 9	$L_u(z_2,\lambda)$	5		7 – 9	
10	$L_u(\lambda)$ Dark	--		10	
11	$E_s(\lambda)$ Dark	--	1	11	
12 – 14	$E_s(\lambda)$	0^+	2 – 4	12 – 14	
15	$E_s(\lambda)$ Dark	--	5	15	
16	$L_u(\lambda)$ Dark	--	6		
17 – 19	$L_u(z_1,\lambda)$	1	7 – 9		
20	$L_u(\lambda)$ Dark	--	10		
21	$E_s(\lambda)$ Dark	--	11		1
22 – 24	$E_s(\lambda)$	0^+	12 – 14		2 – 4
25	$E_s(\lambda)$ Dark	--	15		5
26	$L_u(\lambda)$ Dark	--			6
27 – 29	$L_u(z_3,\lambda)$	9			7 – 9
30	$L_u(\lambda)$ Dark	--			10
31	$E_s(\lambda)$ Dark	--			11
32 – 34	$E_s(\lambda)$	0^+			12 – 14
35	$E_s(\lambda)$ Dark	--			15